Ocean Heat Transport and Water Vapor Greenhouse in a Warm Equable Climate: A New Look at the Low Gradient Paradox

Citation: Rose, Brian E. J., and David Ferreira. "Ocean Heat Transport and Water Vapor Greenhouse in a Warm Equable Climate: A New Look at the Low Gradient Paradox." Journal of Climate 26, no. 6 (March 2013): 2117-2136. © 2013 American Meteorological Society

As Published: http://dx.doi.org/10.1175/JCLI-D-11-00547.1

Publisher: American Meteorological Society

Persistent URL: http://hdl.handle.net/1721.1/80782

Version: Final published version: final published article, as it appeared in a journal, conference proceedings, or other formally published context

Ocean Heat Transport and Water Vapor Greenhouse in a Warm Equable Climate: A New Look at the Low Gradient Paradox

BRIAN E. J. ROSE

Department of Atmospheric Sciences, University of Washington, Seattle, Washington

DAVID FERREIRA

Department of Earth, Atmospheric and Planetary Sciences, Massachusetts Institute of Technology, Cambridge, Massachusetts

(Manuscript received 26 September 2011, in final form 12 April 2012)

ABSTRACT

The authors study the role of ocean heat transport (OHT) in the maintenance of a warm, equable, ice-free climate. An ensemble of idealized aquaplanet GCM calculations is used to assess the equilibrium sensitivity of global mean surface temperature ($\overline{T}$) and its equator-to-pole gradient (ΔT) to variations in OHT, prescribed through a simple analytical formula representing export out of the tropics and poleward convergence. Low-latitude OHT warms the mid- to high latitudes without cooling the tropics; $\overline{T}$ increases by 1°C and ΔT decreases by 2.6°C for every 0.5-PW increase in OHT across 30° latitude. This warming is relatively insensitive to the detailed meridional structure of OHT. It occurs in spite of near-perfect atmospheric compensation of large imposed variations in OHT: the total poleward heat transport is nearly fixed.

The warming results from a convective adjustment of the extratropical troposphere. Increased OHT drives a shift from large-scale to convective precipitation in the midlatitude storm tracks. Warming arises primarily from enhanced greenhouse trapping associated with convective moistening of the upper troposphere. Warming extends to the poles by atmospheric processes even in the absence of high-latitude OHT.

A new conceptual model for equable climates is proposed, in which OHT plays a key role by driving enhanced deep convection in the midlatitude storm tracks. In this view, the climatic impact of OHT depends on its effects on the greenhouse properties of the atmosphere, rather than its ability to increase the total poleward energy transport.

1. Introduction

One of the most vexing puzzles in the paleoclimate record has been the apparent dominance of warm, equable climates over long periods of Earth's history. The climates of the Cretaceous and the early Eocene would be quite unrecognizable to us, particularly in the polar regions. Eocene vegetation records from high-latitude continental interiors indicate warm, frost-free conditions even in winter (e.g., Greenwood and Wing 1995), while deep ocean temperatures (presumably set at the high latitude sea surface) were much warmer than at present (Zachos et al. 2001). These ice-free periods are characterized as having a warmer global mean temperature $\overline{T}$ and reduced equator-to-pole temperature gradient ΔT. The term ''equable'' typically refers to both the weak meridional ΔT and reduced seasonality.

Weak ΔT during warm periods has proven difficult to reconcile with climate model results, inspiring related puzzles known as the ''equable climate problem'' and the ''low gradient paradox'' (Huber and Caballero 2011). We characterize the low gradient paradox as follows: weak ΔT seems to demand increased poleward heat transport, while simultaneously implying weak poleward heat transport, since much of the transport in the present climate is effected by atmospheric eddies resulting from baroclinic instability (see e.g., Barron 1983, 1987; Lindzen 1994; Huber and Sloan 2000; Hotinski and Toggweiler 2003; Korty et al. 2008).

The weakness of ΔT during past warm periods is poorly constrained. Tropical SST reconstructions are subject to a number of ambiguities in the interpretation of proxy data (Huber 2008; Zhou et al. 2008). Once thought to be

Corresponding author address: Brian Rose, Department of Atmospheric Sciences, University of Washington, Box 351640, Seattle, WA 98195.
E-mail: brose@atmos.washington.edu

DOI: 10.1175/JCLI-D-11-00547.1

somewhat cooler than at present (e.g., D'Hondt and Arthur 1996), modern estimates now put tropical SSTs several degrees warmer than present, both in the early Eocene (Pearson et al. 2007) and mid-Cretaceous (Norris et al. 2002; Wilson et al. 2002). Large uncertainties in these estimates persist, making it difficult to rule out the possibility these warm periods were driven by a simple increase in CO_2 (Huber and Caballero 2011). Here we suppose that there is a genuine low gradient paradox to be resolved and offer some new dynamical insight into this long-standing problem. Even should the "hot tropics" view of the Eocene prevail in future reconstructions, alternative mechanisms for warm-pole climates that could operate in the absence of elevated CO_2 would be of great interest, given the prevalence of ice-free conditions throughout the Phanerozoic (e.g., Royer et al. 2004).

Increased ocean heat transport (OHT) from low to high latitudes as a potential resolution of the low-gradient paradox is a long-running theme in the literature—see, for example, Covey and Barron (1988), Sloan et al. (1995), Schmidt and Mysak (1996), Bice et al. (2000), and reviews therein. OHT is completely unconstrained by paleoclimatic data (Bice et al. 2000), making it a prime candidate for speculation and creative thinking. This paper focusses on the atmospheric processes setting $\overline{T}$ and ΔT in response to variations in OHT in warm climates, and does not deal explicitly with the oceanic mechanisms for such variations. However, a few words are in order about the plausibility of our experiments in a paleoclimate context.

One proposed mechanism for increased OHT in warm climates is enhanced mixing through the thermocline by tropical cyclones (Emanuel 2002; Korty et al. 2008), though its effectiveness has been questioned (Jansen and Ferrari 2009; Jansen et al. 2010). Another possibility is that tectonic rearrangement of tropical landmasses has driven changes in ocean circulation. Hotinski and Toggweiler (2003) point out that the equable Cretaceous climate coincided with a tropical circumglobal oceanic passage (the Tethyan gap). The opening of a tropical seaway in their model allows for enhanced wind-driven equatorial upwelling of cold abyssal water (in analogy with oceanic processes in the present-day Southern Ocean), a consequent 1 PW increase in OHT and order 5°C warmer extratropical SSTs. Enderton and Marshall (2009) find consistent results in a fully coupled general circulation model (GCM): opening an equatorial passage increases OHT by order 0.5–1 PW and warms the poles by 5°C. The increase in OHT is attributed both to the absence of equatorial gyres (which transport heat equatorward, Hazeleger et al. 2004) and to deeper tropical upwelling.

These experiments with idealized basin geometries may represent upper bounds on the sensitivity of OHT to tectonic changes. Many earlier works investigated the effects of realistic paleogeographies with uncoupled ocean models but suffer from logical and physical inconsistencies associated with the need to specify sea surface boundary conditions (see review by Huber et al. 2003). Fully coupled models have tended to show rather modest sensitivity of OHT to different paleogeographies (e.g., Huber and Sloan 2001; Huber and Nof 2006; von der Heydt and Dijkstra 2006; Zhang et al. 2011); none of these works report OHT variations greater than 0.5 PW. However they deal with various Cenzoic paleogeographies that do not feature a prominent circumtropical seaway. To our knowledge the only explicit comparison between Cretaceous and present-day coupled model simulations is by Otto-Bliesner et al. (2002), who show OHT changes in excess of 1 PW.[1] More fundamentally, Hotinski and Toggweiler (2003) argue that the tropical upwelling depth in the absence of meridional boundaries is sensitive to numerical details and is probably underestimated in most GCMs because of spurious momentum losses in the ocean interior. A thorough test of this assertion in the presence of detailed and realistic paleogeography has yet to be performed.

One can ask why the climate system ought to care at all about variations in OHT. From theoretical arguments, Stone (1978) found that the total poleward heat transport (THT) is nearly fixed by the planetary albedo and astronomical parameters and is largely insensitive to the detailed atmospheric and oceanic processes that effect the transport. Climate modelers from Manabe (1969) to the present (e.g., Enderton and Marshall 2009) have found nearly complete compensation by atmospheric heat transport (AHT) as mechanisms of OHT are varied in coupled models. Vallis and Farneti (2009) argue that compensation is not a fundamental feature of atmosphere–ocean coupling, but results from the high dynamical efficiency with which the atmosphere responds to temperature gradients.[2] There is no compelling reason to expect the efficiency of AHT to have been weaker during past warm climates; efficiency may in fact increase with warming due to the increasingly important role of latent heat transport (Pierrehumbert 2002; Caballero and Langen 2005; Held and Soden 2006).

Efficient atmospheric compensation presents a significant hurdle to the "enhanced OHT" hypothesis of

[1] An early coupled Cretaceous simulation by Bush and Philander (1997) was integrated for only 32 years and does not provide insight into interior ocean processes. Zhou et al. (2008) report on oxygen isotope distributions and give little information about circulation and heat transport in their simulations.

[2] This efficiency is weaker, for example, at higher planetary rotation rate (Vallis and Farneti 2009).

equable climates (e.g., Barron 1987; Covey and Barron 1988; Rind and Chandler 1991). If THT is roughly fixed, and if surface temperatures are strongly coupled to top-of-atmosphere (TOA) radiative budgets, it follows that a change in OHT should not have much effect on temperatures. However, a reorganization in the atmosphere–ocean partition of heat transport may entail a change in the surface energy budget. The most well-known example is the sensitivity of sea ice extent to OHT, with its consequent effects on albedo. Much previous work on the climatic impacts of OHT have focused on its effects on sea ice (Rind and Chandler 1991; Barron et al. 1993; Seager et al. 2002; Winton 2003). Even in the absence of ice and snow, coupled models have shown that an increase in OHT can reduce ΔT substantially, despite near-zero changes in THT (e.g., Enderton and Marshall 2009). The reasons for this sensitivity have never been properly elucidated. Closely related to the low-gradient paradox, therefore, is the problem of explaining how OHT can warm the poles without altering the TOA energy budget. This is the main focus of the present paper.

In the present climate, the oceans dominate the THT out of the deep tropics, but contribute only a small fraction in the mid to high latitudes (Trenberth and Caron 2001; Wunsch 2005). The meridional structure of OHT (most of the convergence occurring in subtropical to midlatitudes) is thought to be a key feature of the ocean–sea ice interaction in cold climates (Rose and Marshall 2009; Ferreira et al. 2011, hereafter FMR11). In the context of warm climates, we are aware of no previous study that has considered the relative importance of the large amounts of OHT out of the tropics, versus the small transport directly into the polar regions. A large part of the tropical OHT results from robust wind-driven effects (Held 2001; Czaja and Marshall 2006; Vallis and Farneti 2009; FMR11), whereas the heat transport at high latitudes is subject to subtle details of continental configuration and the hydrological cycle and has likely varied greatly over time.

In this study we restrict attention to warm, ice-free climates, and investigate the climatic impact of OHT using an atmospheric GCM coupled to a slab mixed-layer ocean model with prescribed OHT. The imposed OHT variations span a wide range of meridional shapes and sizes (see section 2) but are specified via a simple geometrical formula. These variations are large and are not meant to represent any particular geological event. We emphasize that we are not simulating the climate of a particular period in Earth's history but rather aiming to build an understanding of the fundamental role of OHT in warm climates. We therefore keep the experimental setup as simple as possible, which will also allow for easier replication with other models. Key questions include the following. How do variations in OHT (magnitude and meridional scale) affect $\overline{T}$ and ΔT? To what extent does AHT compensate for changes in OHT? Can OHT warm the poles without extending into high latitudes? What are the mechanisms by which changes in low-latitude OHT are communicated to the poles? How can we reconcile compensation of heat transport with the apparent sensitivity of surface climate to OHT?

Many clues can be found in the literature. Herweijer et al. (2005) find that OHT exerts a global warming in the present climate, only some of which is attributed to sea ice retreat. A key component of the warming is driven by a dynamical moistening and redistribution of water vapor. OHT weakens the Hadley circulation, allowing moist convection to spread out of the deep tropics into its flanks, which moistens the subtropical troposphere and allows for increased greenhouse trapping. In the low latitudes, the oceanic redistribution of heat is felt through a deep tropospheric layer by means of moist convection, with important consequences for the radiative budget. In the more stably stratified midlatitudes, their results show a secondary peak in moistening and warming, but the extratropical effects appear to be less robust between models (and tightly coupled to sea ice effects).

In warm, ice-free climates, the thermal stratification of the extratropical atmosphere likely differed significantly from the present. Korty and Emanuel (2007) and FMR11 find moist-adiabatic tropospheric lapse rates at all latitudes and all seasons in GCM simulations with weak ΔT. This underlines a potentially crucial dynamical distinction of warm climates, namely that extratropical moist convection plays a key role in regulating the climate. Observational analyses show that moist-neutral, convectively adjusted air masses are in fact common in the extratropics today (Korty and Schneider 2007), but largely confined to continental interiors in summer and oceanic storm tracks in winter. Deep convection driven by ocean heating has been observed over the Gulf Stream (Minobe et al. 2008) and is argued to be the primary mechanism by which the oceanic signal is communicated to the free troposphere, though slantwise (as opposed to vertical) moist convection may be a dominant process in the present-day midlatitudes (Korty and Schneider 2007; Czaja and Blunt 2011). In all likelihood, moist convection was even more widespread during warm climates.

Abbot and Tziperman (2008a) identified a potentially important role for polar convection in the maintenance of equable climates. They focus on winter over polar oceans, where the radiative forcing of deep clouds is unambiguously positive. In the absence of sea ice, heat

flux through the relatively warm sea surface can destabilize the polar atmosphere and give rise to optically thick clouds, thereby insulating the sea surface and preventing sea ice formation. The feedback has been demonstrated in a range of models (Abbot and Tziperman 2008a,b; Abbot et al. 2009b,a). They do not discuss variations in OHT, but the onset of convection is clearly sensitive to the ocean-to-atmosphere heat flux (Abbot and Tziperman 2009).

Putting these lines of evidence together, and in anticipation of our model results, we suppose the following: if a warm, equable climate with convectively adjusted atmosphere were subject to an increase in OHT out of the tropics, the increased heating at the midlatitude sea surface would tend to destabilize the atmosphere and trigger increased moist convection. The signal would be felt through a deep tropospheric layer as a roughly uniform warming. In the tropics (where the dynamical regime is not distinctly different from the present-day), the response might look similar to that found by Herweijer et al. (2005): a weakening of the Hadley cells, partially compensating short- and longwave cloud changes and an overall modest temperature change. There may thus be a reduction in the temperature gradient between the tropics and midlatitudes, and a consequent reduction in AHT compensating for the increased OHT. The ultimate fate of the initial midlatitude warming, in the face of reduced AHT, depends crucially on the radiative implications of the increase in moist convection. It has been argued that convection warms the subtropics (Herweijer et al. 2005) and the poles (Abbot and Tziperman 2008a); we therefore expect it also to warm the midlatitudes, both by replacing low stratiform cloud with high cloud, and through injection of water vapor into the dry upper troposphere. Finally, AHT into the polar regions may decrease or increase depending on the detailed meridional structure of OHT. If OHT extends only into midlatitudes, the atmosphere will respond to the increased mid- to high-latitude temperature gradient by fluxing additional warm, moist air to the poles.

Conversely, a reduction in OHT out of the tropics might lead to a stabilization of the extratropical atmosphere, such that extratropical convection is suppressed. The radiative cooling associated with loss of tropospheric water vapor and high cloud might then allow the poles to cool and freeze over even in the presence of a compensating increase in AHT.

The rest of this paper will examine the feasibility of the above scenario in detail. Section 2 describes the numerical model and the imposed OHT variations. Results of the numerical calculations are discussed in section 3. In section 4 we present a very simple two-box model encapsulating the key physics linking OHT and surface temperature, as diagnosed from the GCM. A discussion and conclusions follow in sections 5 and 6, and some parameter sensitivity tests are described in the appendix.

2. Experimental setup

a. Model description

We use an atmospheric GCM coupled to a 60-m aquaplanet mixed layer ocean with a prescribed source/sink term representing the local convergence of OHT, that is, a ''q-flux.'' The model setup is very similar to that used in Section 4 of FMR11.

The model is of ''intermediate'' complexity, using the MIT general circulaton model (MITgcm) dynamical core (Marshall et al. 1997, 2004) on the cubed-sphere grid (Adcroft et al. 2004) at C24 horizontal resolution (24×24 points per face, yielding a resolution of 3.75° at the equator). The atmosphere has five vertical levels and physical parameterizations based on the Simplified Parameterizations, Primitive-Equation Dynamics (SPEEDY) model (Molteni 2003). These include a four-band longwave radiation scheme (two water vapor channels, a ''window'' region, and a CO_2 band with transmissivity tuned to present-day pCO_2), diagnostic clouds, a boundary layer scheme, and parameterizations for moist convection and large-scale precipitation. Resolution is sufficient to simulate baroclinic instability and develop a vigorous storm track. It is forced by seasonally varying solar radiation with default modern-day solar luminosity and obliquity. Eccentricity is set to zero to preserve interhemispheric symmetry. The same atmospheric model was used in a fully coupled setup by Ferreira et al. (2010) and FMR11, with closely related models used in Marshall et al. (2007) and Enderton and Marshall (2009) [see Ferreira et al. (2010) for key differences].

The large-scale condensation scheme generates precipitation wherever relative humidity (RH) exceeds a vertically dependent threshold value, relaxing RH toward this threshold with a time scale of 4 h. Threshold value is 90% at the surface and decreases slightly with height. Any condensed water is assumed to rain out immediately. Moist convection is a simplified version of the mass flux scheme developed by Tiedtke (1989). It represents transport of water vapor and dry static energy by updrafts of saturated air from the boundary layer and compensating large-scale descent. The scheme is activated whenever saturation moist static energy increases vertically, and boundary layer humidity exceeds threshold conditions on either specific humidity or RH. Mass fluxes are determined by treating the convective drying of the boundary layer as a relaxation toward the humidity threshold with a 6-h time scale. Entrainment into the

updraft occurs in the lower troposphere, while detrainment (and therefore latent heat release) is assumed to occur only at cloud top. The scheme is described in more detail in the appendix, along with some sensitivity tests with altered parameter values.

Molteni (2003) compares ensembles of SPEEDY simulations driven by observed SSTs to 41 years of reanalysis data. The climatology of precipitation is on par with more complex GCMs. The boreal winter distribution of precipitation is quite realistic; boreal summer precipitation is biased toward a weak South Asian monsoon associated with a midtropospheric cold bias. Bracco et al. (2004) find that biases in SPEEDY simulations are further reduced by prescribing an increase in CO_2 optical depth consistent with observed trends in CO_2 concentration. An 8-level version of SPEEDY has recently been coupled to a global ocean model with realistic geography by Severijns and Hazeleger (2010); they find a warming of 3.2 K for a doubling of CO_2, within the range of climate sensitivities exhibited by high-end coupled models. These studies suggest that the SPEEDY parameterizations (and therefore our aquaplanet GCM) represent fundamental radiative and moist physical processes sufficiently realistically to provide a useful tool for exploration of climate mechanisms.

The aquaplanet model is known to exhibit multiple states (FMR11). Sea ice forms when the polar oceans reach the freezing point, and the climate rapidly cools into a qualitatively different state. In this paper we report only on the warm, ice-free state of the model. In the absence of sea ice, the surface albedo is low and varies only with solar zenith angle. Analogous experiments investigating the role of OHT in mediating sea ice cover, and the existence of multiple equilibria, will be reported elsewhere.

b. The prescribed OHT

In Fig. 1 we overlay six different plots of OHT (zonal, annual mean) to give a sense of its dynamic range across widely different climates: two observationally based estimates from Trenberth and Caron (2001) and four curves from the coupled aquaplanet GCM calculations of FMR11. These are simulations under two different, highly idealized continental configurations (with and without a pole-to-pole ''ridge'' bounding the ocean into a global basin), each of which permits both a warm ice-free climate and a much colder climate with extensive sea ice cover. The general shape of the curve in all cases is a large peak of poleward heat transport out of the deep tropics in each hemisphere and convergence in the subtropics to midlatitudes. Reasons for this robust structure of OHT across models and observations are discussed by Enderton and Marshall (2009) and FMR11. Figure 1 shows variations in both the magnitude of the peak tropical transport and the width of the high latitude

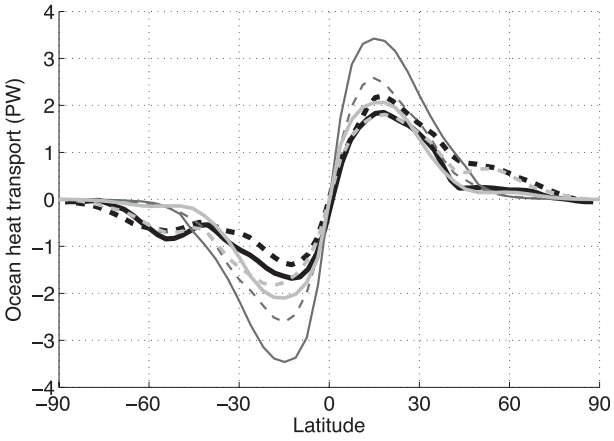

FIG. 1. Ocean heat transport from observations and aquaplanet models. Thick black curves are two estimates of present-day OHT from Trenberth and Caron (2001). Others are OHT from the four different coupled aquaplanet GCM calculations reported in Ferreira et al. (2011) (FMR11)—the Warm (light gray) and Cold (dark gray) states of the Aquaplanet (solid) and Ridgeworld (dashed). See FMR11 for details.

tail—that is, how much heat of tropical origin is carried into the higher latitudes.

These variations inspire a simple analytical form for the OHT in these model experiments:

$$\mathrm{OHT} = \Psi \sin(\phi)\cos(\phi)^{2N} = \Psi x(1-x^2)^N, \qquad (1)$$

where $x = \sin\phi$ and ϕ is latitude, N is a positive integer, and Ψ is a constant (in units of watts) setting the amplitude. OHT and its convergence computed from Eq. (1) are plotted in Fig. 2 for values of N ranging from 1 to 8, with Ψ scaled in each case to give a peak transport of 2 PW. All q-fluxes used here are steady in time and zonally symmetric.

Here, N and Ψ are the two control parameters in these experiments, setting the meridional scale and amplitude of OHT. From the lower panel of Fig. 2, the q-flux acts to cool the deep tropics in all cases. Convergence (heating) occurs over a range of subtropical to midlatitudes, shifting equatorward for larger values of N. The forcing is conservative in all cases, acting only to redistribute energy within the ocean mixed layer.

Note that the forcing goes to zero (no heating) at the poles in most cases. The exception is $N = 1$, for which OHT has a broad equator-to-pole structure, with maximum convergence at the poles. This is not realistic, and will turn out to be an outlier in our simulations, but is included for the sake of a more complete exploration of the OHT parameter space.

We vary the peak amplitude between 1 and 4 PW. In all cases the model is initialized in a warm-pole state (taken from FMR11), and integrated out to quasi-equilibrium. Those runs that experience sea ice growth

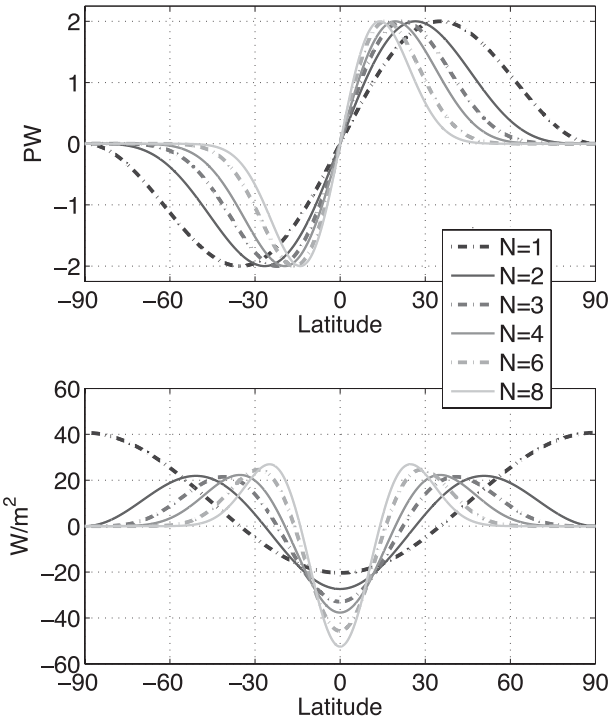

FIG. 2. (top) Idealized OHT (in PW) and (bottom) its convergence (in W m^{-2}) computed from the analytical Eq. (1) for various values of the scale parameter N (amplitudes are adjusted such that all transport curves have peak values ± 2 PW).

are excluded from the analysis (including $N = 3$, 4, 6 at 1 PW and $N = 8$ at 1 and 2 PW). All results presented below are based on 20-yr averages.

This modeling study is distinct from that of Herweijer et al. (2005) for several reasons. By restricting attention to ice-free climates, we avoid complications associated with differing treatments of sea ice. More fundamentally, the absence of strong thermal stratification near the poles in our warm simulations plays a key role in the atmospheric response to OHT variations (to be shown below). We also explore a larger span of OHT changes, and systematically separate changes in amplitude versus meridional extent of OHT.

3. Results

a. Surface temperature

Figure 3 shows the zonal, annual mean surface air temperature as a function of the imposed q-flux.[3] Results are grouped into panels by meridional scale parameter N, with different amplitudes shown in colors in each panel. Tropical temperatures vary by no more than a few degrees Celsius over the entire ensemble, while polar temperatures span 20°C. We note the following:

- $\overline{T}$ increases with OHT amplitude;
- the warming is polar-amplified, by a factor of 3;
- the largest temperature differences are felt at the poles, regardless of the meridional extent of the OHT; and
- ΔT weakens as OHT increases.

In fact the equator-to-pole temperature structure seems to follow a universal scaling in these simulations, as shown in Fig. 4. Here we plot ΔT versus $\overline{T}$ for the entire ensemble (ΔT is calculated from zonal mean surface air temperatures directly at the equator and pole). The relationship is remarkably linear: ΔT decreases by 2.6°C for every 1°C increase in $\overline{T}$.

These results suggest surface temperatures are sensitive to both amplitude and meridional scale of OHT, in roughly equivalent ways. This is illustrated in Fig. 5, in which we plot the polar temperature T_{pole} as a function of OHT across fixed latitudes. The correlation is positive in all cases, but the best fit appears to be at 30° latitude, with most of the results collapsing onto a single line: T_{pole} increases by 4.6°C per PW carried poleward across 30° by the oceans. The climate system appears to be relatively insensitive to the detailed meridional distribution of OHT convergence, but broadly sensitive to the oceanic energy flux into the midlatitudes. We note that 30° is approximately the poleward edge of the Hadley cells. According to this scaling, the poles will drop below 0°C when the oceans carry less than about 0.5 PW across 30° latitude. Consistently, we find that sea ice forms in the GCM with 1 PW peak OHT and $N > 2$ (such that the peak occurs equatorward of 30°—see Fig. 2).

The outliers in Fig. 5 are for $N = 1$, which produces more polar warming per unit OHT across 30°. However the close scaling of $\overline{T}$ and ΔT in Fig. 4 still applies in this case.

b. Compensation of heat transport

Changes in AHT compensate nearly completely for imposed changes in OHT in these simulations, as shown in Fig. 6. The upper panel shows the entire ensemble of imposed OHT curves (shades of gray), and the resulting total heat transport curves (THT = AHT + OHT) in blue. AHT is computed directly from statistics of moist static energy fluxes in the GCM.[4] THT is computed as

[3] Differences between surface air temperature and SST are small, never exceeding 2°C in these simulations.

[4] AHT is well approximated by the flux of moist static energy, defined as MSE = $c_pT + gz + Lq$ (notation standard), which can be further decomposed into dry static energy DSE = $c_pT + gz$ (the sum of internal and potential energy) and latent heat LH = Lq (Pierrehumbert 2010).

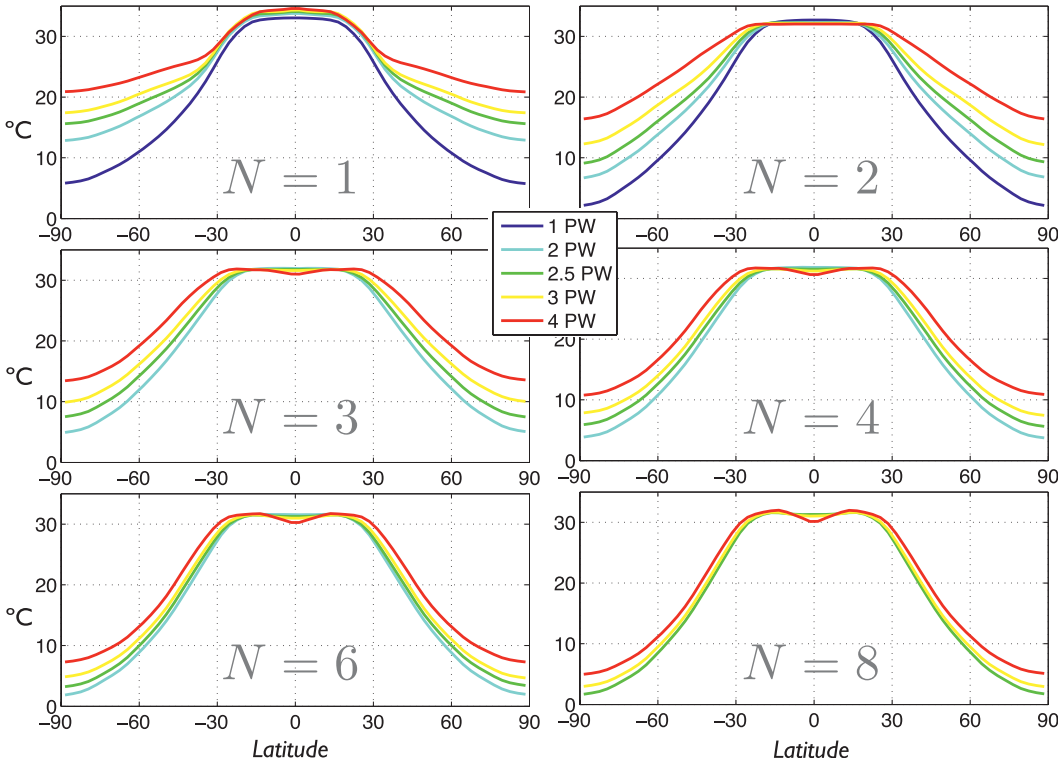

FIG. 3. Surface air temperature (zonal, annual mean) vs latitude as a function of OHT scale and amplitude. Each panel has a fixed meridional scale parameter N, with amplitudes indicated by the color scale.

the sum of this AHT and the imposed OHT as given in Eq. (1). These curves therefore represent very accurate measures of the total heat transport in the model, independent of TOA radiative fluxes. Peak THT is remarkably similar to its present-day value of nearly 6 PW in all cases (Trenberth and Caron 2001). Variations in THT at its peak near 35° are less than 0.2 PW, despite the 3-PW range of the prescribed OHT.

The lower panel of Fig. 6 shows the change in THT as OHT increases from 2 to 3 PW, as a function of N.[5] THT anomalies range from negative (i.e., overcompensation by AHT) for large-scale OHT (small N) to positive (undercompensation by AHT) for small-scale OHT (large N). We emphasize that polar-amplified climate warming occurs in all these cases, regardless of the sign of the change in THT. In fact the greatest polar warming (or decrease in ΔT) occurs in association with a *reduction* in THT (e.g., for $N = 1$ and 2). The important implication of these results is that the high-latitude warming is *not* fundamentally driven by an increase in the poleward energy transport of the atmosphere–ocean system.

Figure 7 shows the components of AHT across 45° (roughly at its peak), decomposing the total flux of moist static energy (MSE) into dry static energy (DSE) and latent heat (LH). These are plotted against $\overline{T}$ in the left

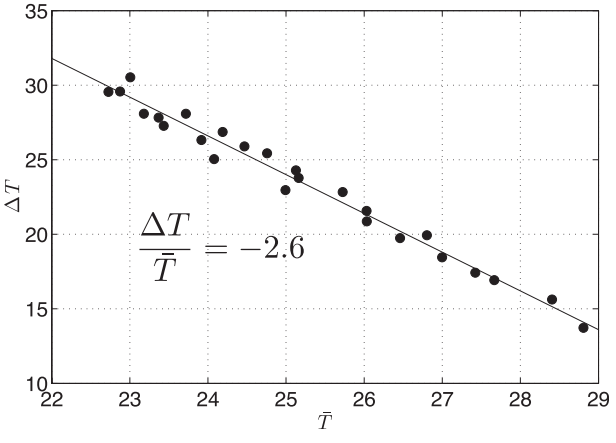

FIG. 4. Equator-to-pole temperature gradient ΔT vs global mean temperature $\overline{T}$ for the entire array of warm climates plotted in Fig. 3. Best-fit line $\Delta T = -2.6\overline{T} + 89$ is indicated, with temperatures in °C.

[5] For $N = 8$ the anomaly from 2.5 PW to 4 PW OHT is shown instead, since in this case the model grows large sea ice caps with only 2 PW OHT.

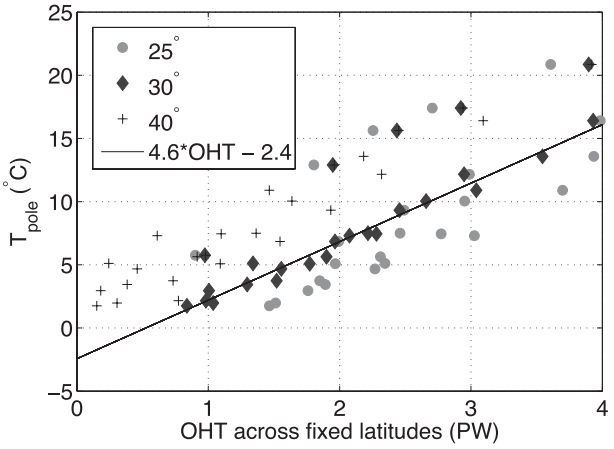

FIG. 5. Polar temperature as function of OHT across fixed latitudes. The black line is the best fit to OHT30, excluding the five points from $N = 1$.

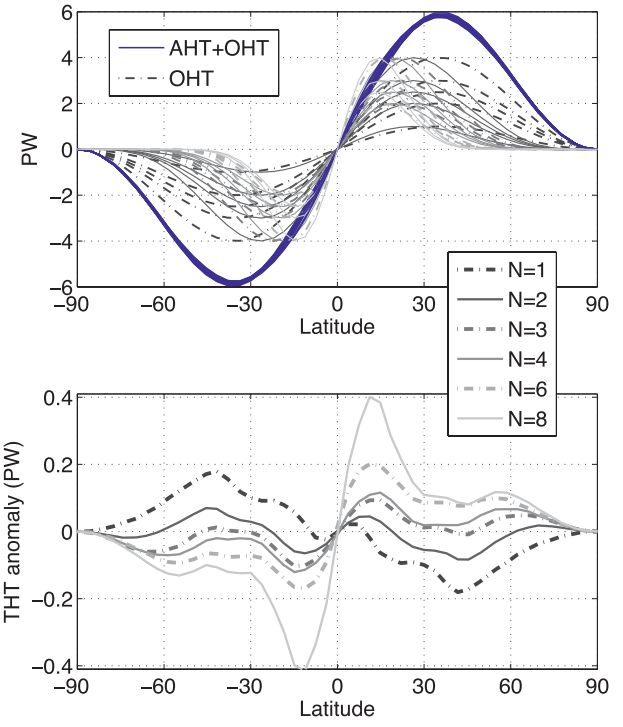

FIG. 6. (top) The full range of OHT prescribed in the GCM (gray lines), and resulting total heat transport (THT = OHT + AHT) for the 25-member ensemble of model runs (blue lines). (bottom) THT anomaly as OHT amplitude increases from 2 to 3 PW, as a function of the meridional scale parameter N. (For $N = 8$, the anomaly from 2.5 PW to 4 PW OHT is shown, since 2 PW OHT is insufficient to prevent sea ice formation in this case).

panel. There is a wide scatter in the response, but we note that both LH and DSE fluxes tend to decrease as OHT increases and the climate warms. This is consistent with the results of Caballero and Langen (2005), who find that in the warm, weak gradient regime, LH transport tends to be roughly constant with $\overline{T}$ and proportional to ΔT, thus decreasing slightly as the poles warm. It should be noted, however, that the spatial structures of these fluxes are complex, and the relative importance of LH versus DSE varies substantially at different latitudes. Closer to the pole, we find an increase in the LH component as the climate warms (not shown).

The primary compensation mechanism appears to be a reduction in storm track intensity as OHT increases, the climate warms and ΔT decreases. In the right panel of Fig. 7 we plot the AHT components against an eddy velocity scale V. This scale is estimated from $V = \sqrt{2\overline{\mathrm{KE}}}$, where $\overline{\mathrm{KE}}$ is the eddy kinetic energy at 775 hPa, averaged between 30° and 60° latitude. Again, this result is

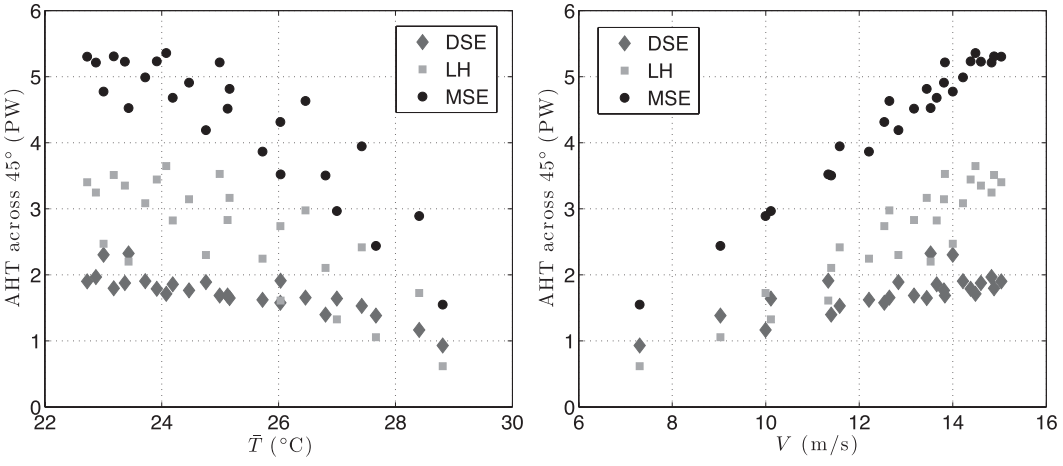

FIG. 7. Components of AHT across 45°. The total flux of moist static energy (MSE) is decomposed into fluxes of dry static energy (DSE) and latent heat (LH), and plotted against (left) $\overline{T}$ and (right) V (right), an estimate of eddy velocity scales in the midlatitude storm track.

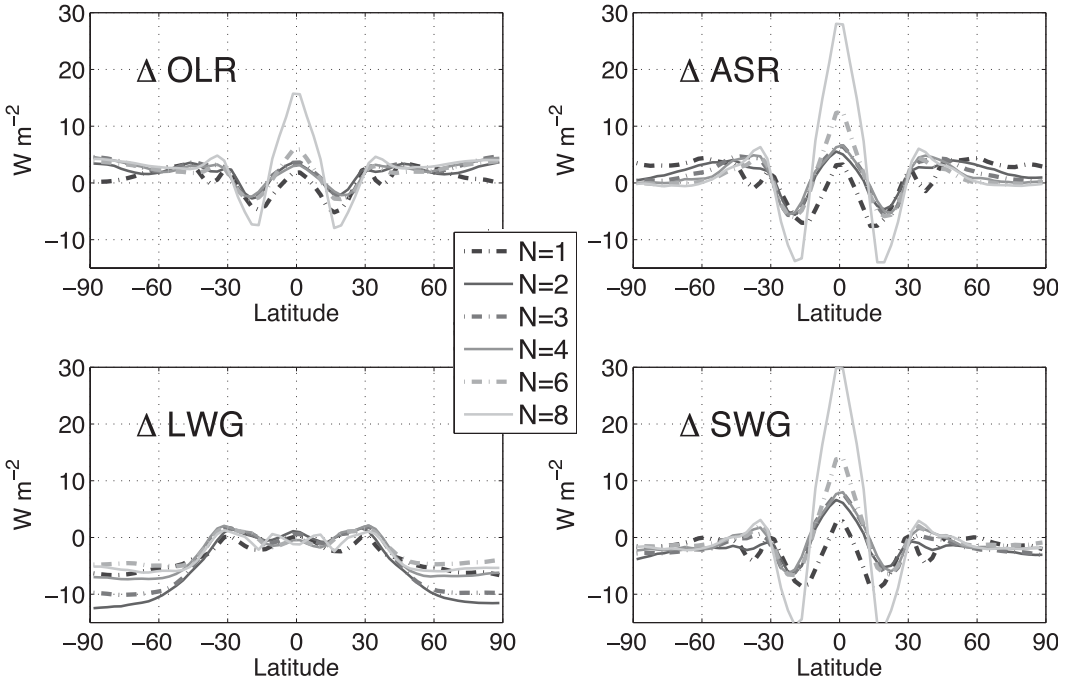

FIG. 8. Radiative flux anomalies as OHT increases from 2 to 3 PW (except for $N = 8$, as in Fig. 6). (top left) OLR at TOA. (top right) ASR—difference between incident and outgoing shortwave at TOA. (bottom left) Net upward longwave flux at surface. (bottom right) Net downward shortwave flux at surface.

consistent with Caballero and Langen (2005) in the warm, weak gradient regime. The damping of baroclinic instability as ΔT weakens overwhelms any increase in moisture supply (and thus potential increases in LH fluxes) as $\overline{T}$ increases.

c. *Radiative forcing*

The surface warming associated with increasing OHT shown in Fig. 3 requires an increase in either absorbed solar radiation (ASR), greenhouse trapping of longwave radiation, or convergence of poleward heat transport (or some combination). We showed in the previous section that heat transport cannot explain the warming. We turn to the radiative forcing in Fig. 8, which shows anomalies in net long- and shortwave fluxes at TOA (upper panels) and the surface (lower panels), for an OHT increase from 2 to 3 PW as a function of N.

We deal first with the tropical radiative balance and the apparent thermostat keeping tropical SSTs within a few degrees despite large variations in OHT. At TOA, in the tropics, there are large, compensating changes in short and longwave budgets. As OHT increases, the Hadley cells weaken and convection tends to spread away from the ITCZ into subtropics (see below for more details). In the deep tropics, the ASR increase due to a reduction in convective cloud cover is partly compensated by an increase in outgoing longwave radiation (OLR) associated with reduced humidity and high cloud, while the reverse occurs in the subtropics. The tropical drying can be inferred from the increase in surface shortwave fluxes, which are slightly larger than the ASR changes because of a reduction in water vapor–dependent solar absorption in the tropical atmosphere. The longwave compensation tends to be incomplete, resulting in an anomalous differential heating across the Hadley cells. This is consistent with the heat transport anomalies (Fig. 6)—for larger values of N there is a positive poleward THT anomaly near 10°–15° latitude. That is, when the tropical OHT has a small meridional scale, the atmospheric compensation is incomplete, and an increase in OHT does in fact cool the deep tropics very slightly (Fig. 3).

We interpret this tropical thermostat as resulting from two distinct cancellations.[6] First, as noted above, short and longwave effects tend to oppose each other locally, primarily because the cloud cover is dominated by high

[6] To be clear, this mechanism is distinct from the dynamical ocean thermostat of Clement et al. (1996). They propose that the SST response to a zonally uniform sea surface heating from the atmosphere is damped by anomalous equatorial upwelling. We impose an oceanic heat sink at the equator (enhanced OHT) and find that the tropical SST response is damped by atmospheric processes.

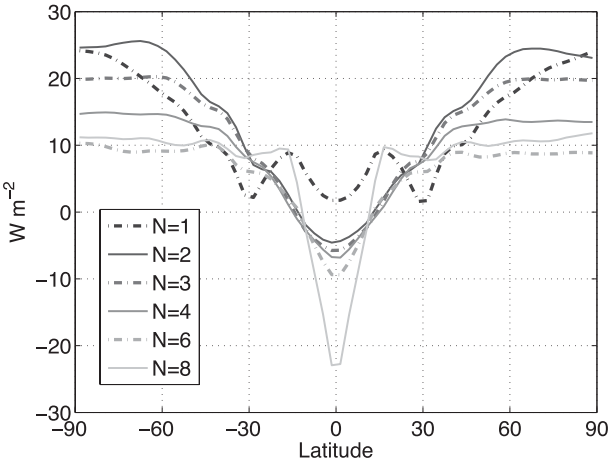

FIG. 9. Anomalies of greenhouse trapping $G_t = \epsilon_s \sigma T_s^4 - \text{OLR}$ as OHT increases from 2 to 3 PW (except for $N = 8$, as in Fig. 6).

convective clouds. Second, changes in net radiation in the deep tropics and the poleward flanks of the Hadley cells are opposite. Since tropical dynamics are subject to a weak temperature gradient constraint (Sobel 2001), these meridional heating gradients are efficiently smoothed out by the atmospheric circulation. The net result is that changes in total radiative forcing within the Hadley cell regime are small. For example, for an increase in OHT from 2 to 3 PW, there is a very small decrease in net radiative heating averaged from the equator to 30°, ranging from 1.3 W m^{-2} for $N = 1$ down to 0.3 W m^{-2} for $N = 6$ (measured from TOA fluxes).

Turning to the extratropics, Fig. 8 shows rather different changes in radiative forcing poleward of 30°. The extratropics receive more net shortwave radiation at TOA, while less of it actually reaches the surface, indicating reduced total cloud cover and increased moisture. There are small increases in OLR, roughly balancing the change in ASR. Thus the net radiative forcing at TOA is largely unchanged, consistent with the small variations in THT (Fig. 6). The biggest signal in Fig. 8 is the decrease in net upward surface longwave flux. This decrease occurs in spite of the surface warming, indicating a substantial increase in the downwelling longwave flux from the atmosphere. In other words, a stronger greenhouse.

Figure 9 shows anomalies in greenhouse trapping, defined as $G_t = \epsilon_s \sigma T_s^4 - \text{OLR}$ following Herweijer et al. (2005), for the same increase in OHT as in Fig. 8.[7] Here, ΔG_t gives a measure of the increase in downwelling longwave at the surface over and above what would be expected solely from the temperature increase. Figure 9 shows that increased greenhouse trapping is the dominant

[7] A surface emissivity of $\epsilon_s = 0.98$ is prescribed in our GCM.

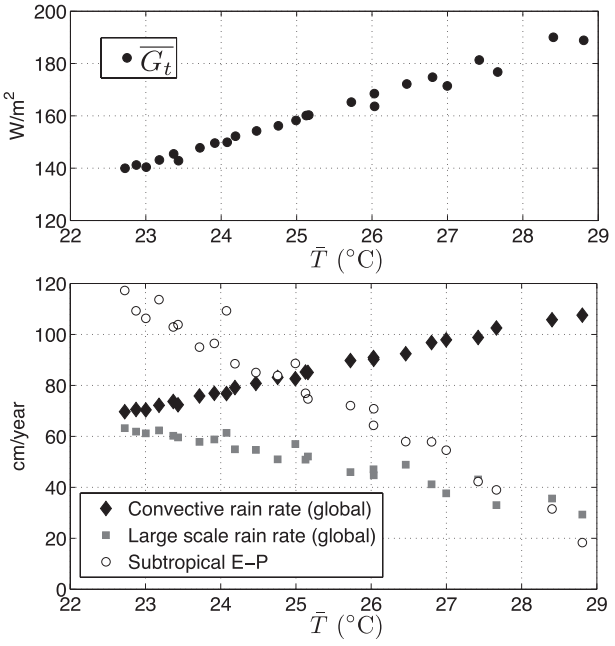

FIG. 10. (top) Scatterplot of extratropical greenhouse trapping $\overline{G_t}$ (averaged poleward of 30°) vs $\overline{T}$. (bottom) Global mean rain rates from convective and large-scale precipitation vs $\overline{T}$. Also plotted is maximum net evaporation minus precipitation in the subtropical dry zone.

term accounting for the extratropical warming. Here, ΔG_t is of order 10 W m^{-2} for large N (small surface warming) and increases to 20–25 W m^{-2} for small N (large surface warming). We argue below that this greenhouse effect is driven by enhanced deep convection in the midlatitude storm tracks. In contrast to the tropics, the longwave forcing is not compensated by an opposite shortwave effect (see ASR plots in Fig. 8). Clouds do not compensate the longwave greenhouse effect here mostly because cloud cover remains high in the storm track regions in all cases. The enhanced deep convection, to be discussed below, means a shift from low to high cloud rather than a substantial change in total extratropical cloud cover.

In Fig. 10 (upper panel) we plot $\overline{G_t}$ averaged poleward of 30° against $\overline{T}$ for the entire ensemble. There is a close positive correlation: warmer climates are associated with more effective extratropical greenhouses, which can be unambiguously attributed to water vapor.

d. Moist convection and water vapor

There is some difficulty in establishing cause and effect in the concomitant increase of temperature and water vapor. Water vapor feedback is usually understood as an amplifier of an external forcing agent (such as CO_2), due to the increase in saturation specific humidity with warming. Thus, at least some of the increase in greenhouse trapping shown in Fig. 10 would be expected under an

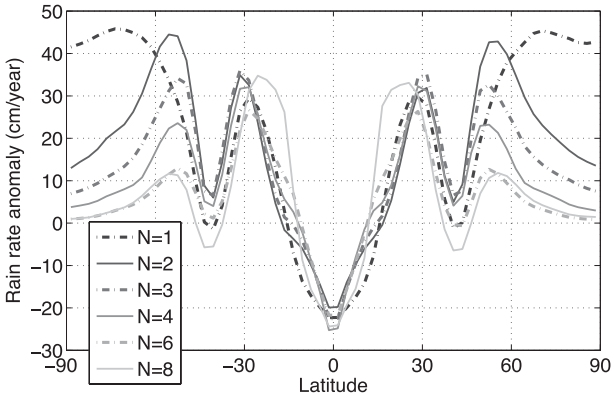

FIG. 11. Convective rain rate anomaly as OHT increases from 2 to 3 PW (except for $N = 8$, as in Fig. 6).

externally driven warming as the atmosphere moistens itself by surface evaporation. However, the radiative impact of water vapor is greatest at high altitudes where it is scarcest, and a comprehensive theory for what sets the tropospheric water vapor distribution is still elusive (Pierrehumbert et al. 2007). A mechanism that moistens the upper troposphere would lead to surface warming via the greenhouse effect; in this case the water vapor would be acting not strictly as feedback but as the primary driver of the surface warming. We argue that this is indeed the case in these simulations, and that deep convection within the midlatitude storm tracks is the moistening mechanism. This is essentially the same argument invoked by Herweijer et al. (2005) to explain subtropical warming due to OHT.

Figure 10 (lower panel) shows a systematic global-mean shift toward more convective precipitation as the climate warms (i.e., as extratropical OHT convergence increases), which is partly offset by a decrease in large-scale precipitation (closely linked to the decrease in the intensity of the midlatitude storm tracks). Figure 11 shows the meridional distribution of the changes in convective rain rate as OHT increases from 2 to 3 PW. There is a shift in convection from the deep tropics to the flanks of the Hadley cells, as noted above, and also found by Herweijer et al. (2005). But there is also a large increase in midlatitude convection. The anomaly is centered on 50° latitude in the heart of the midlatitude storm tracks. The convection anomaly decays (but remains positive) poleward of the storm tracks, except for $N = 1$ where the maximum increase occurs at high-latitudes.

Net evaporation minus precipitation ($E - P$) is also sensitive to variations in OHT. Spatial patterns of $E - P$ anomalies in our simulations are complex and difficult to generalize. However there is one quite robust signal, plotted in Fig. 10: a strong decline of net evaporation in the subtropical dry zones as OHT increases and the climate warms, of order 15 cm yr^{-1} (0.4 mm day^{-1}) per degree of global warming. The increase in subtropical convection shown in Fig. 11 is sufficient to more than offset increased evaporation, such that the dry zones become less dry as the climate warms. Remarkably, this is opposite to the scaling expected under CO_2 warming. Held and Soden (2006) find a robust *increase* of subtropical $E - P$ of order 3 cm yr^{-1} per degree warming in IPCC models. We return to this point in the discussion.

Figure 12 shows the deep structure of the changes in temperature (T), specific humidity (Q), and relative humidity (RH), again plotted as anomalies for an increase in OHT from 2 to 3 PW. The peak warming actually occurs in the midtroposphere within the storm track regions. Temperature changes in the mid-to-high latitudes are roughly uniform in the vertical up to 500 hPa.[8] Because moist adiabatic lapse rates decrease in absolute value at warmer temperatures, this implies that the extratropical thermal stratification approaches moist adiabatic more closely for stronger OHT.

Changes in Q are fairly well coupled to temperature changes, as expected from the Clausius–Clapeyron relation. There are, however, significant variations in RH, which Herweijer et al. (2005) argue can be interpreted as evidence of dynamical mechanisms contributing to a redistribution of water vapor. Several features stand out in the RH anomalies in Fig. 12. The tropical upper troposphere (250 hPa) exhibits a dipole pattern with drying over the equator and moistening near 20°. This pattern gets much stronger at larger N, thus scaling with the magnitude of the oceanic equatorial cooling. The same shift in upper-tropospheric moisture from the equator to the flanks of the Hadley cell was shown by Herweijer et al. (2005), and is linked to the shift in tropical convection discussed above.

In the midlatitudes we find a vertical RH dipole, roughly collocated with the peak warming in the storm-track regions. This pattern features upper-tropospheric (250 hPa) moistening and relative drying of the mid-troposphere (500 hPa), and gets stronger at smaller N, thus scaling with the extratropical convective rain rate anomalies in Fig. 11. We attribute this pattern to an increase in the frequency with which moist convection penetrates to the upper troposphere at these latitudes, since the convection scheme tends to moisten the upper levels and dry out intermediate levels. These patterns of warming and moistening strongly suggests that the OHT signal at the sea surface is communicated deeply into the

[8] Our GCM resolves only 5 levels, so contours in Fig. 12 may exaggerate vertical smoothness of anomalies.

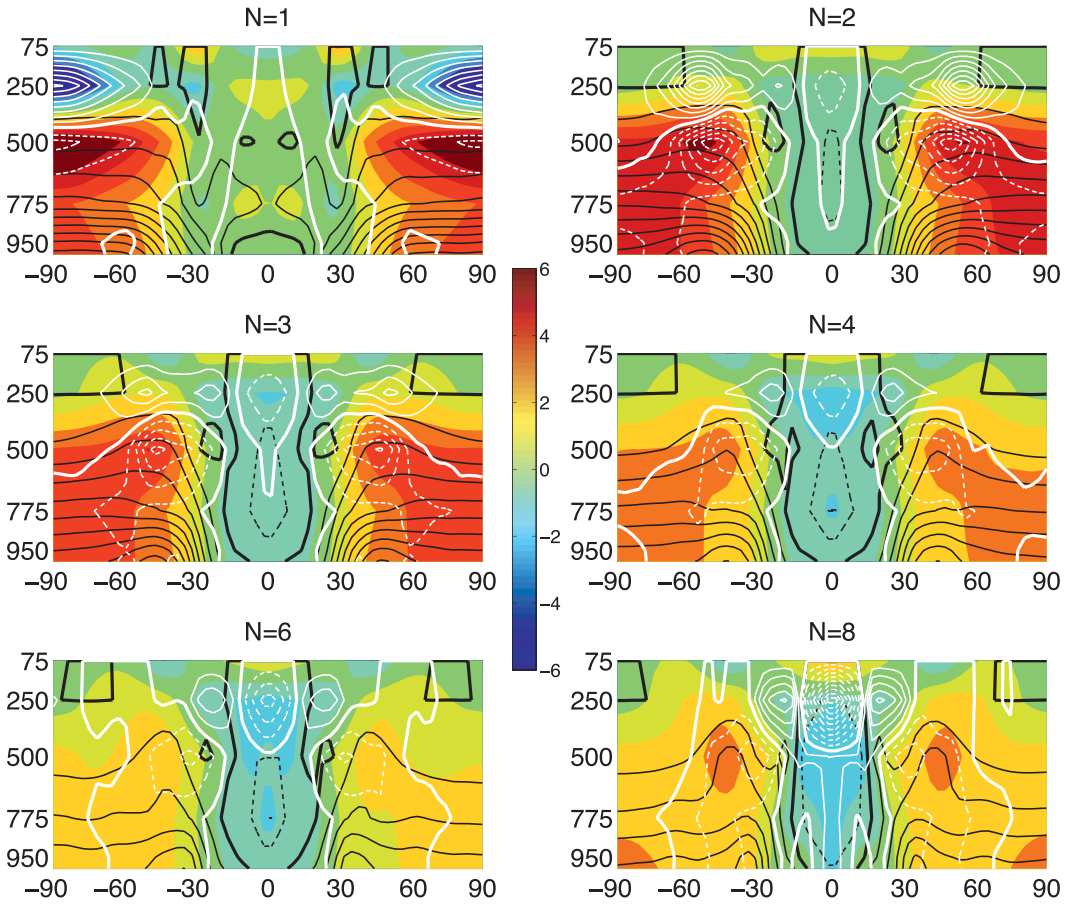

FIG. 12. Latitude–pressure cross sections of temperature and moisture anomalies as OHT increases from 2 to 3 PW (except for $N = 8$, as in Fig. 6). Colors: change in temperature T (color scale ranges from −6 K to +6 K as shown). Black contours: change in specific humidity Q (contour interval 0.25 g kg^{-1}, zero contour bold, negative contours dashed). White contours: change in RH (contour interval 2%, zero contour bold, negative dashed—except for $N = 1$ for which we use an 8% contour interval).

troposphere by moist convection, and that injection of moist air into the upper levels gives rise to the enhanced greenhouse properties shown in Fig. 9.

Here, $N = 1$ is once again an outlier in terms of its warming/moistening pattern. In this case the peaks in warming, convective rain, and upper-tropospheric moistening all occur over the poles rather than the midlatitudes. The very strong increase in RH at 250 hPa over the poles results from both a small absolute moistening (0.05 g kg^{-1}) and a strong local cooling (6°C). RH actually increases from about 20% to 85% in this example.

The peak warming in Fig. 12 shifts equatorward somewhat for higher N (i.e., narrower OHT), but this shift is modest compared to the shift in OHT convergence (Fig. 2), indicating a preference for convection within the midlatitude storm track. Examination of daily GCM output (not shown) reveals that tropical convection is fairly uniformly distributed in space and time, while midlatitude convective rain is patchy and localized within traveling synoptic-scale storm systems, where it can occasionally reach peaks as high as 50 mm day^{-1}. We speculate that the sensitivity of the model climate to OHT across 30° shown in Fig. 5 relates to the degree of sea surface heating occurring within the storm tracks regions, where the atmosphere is most sensitive to this convectively-driven warming.

4. A two-box EBM interpretation

Here we encode some of the ideas presented above into a very simple two-box energy balance model (EBM), in which we solve directly for perturbations in $\overline{T}$ and ΔT in response to specified heat sources and sinks in each box. The model is a slight generalization of the two-box EBM introduced by Langen and Alexeev (2007, hereafter LA07). The two boxes, sketched in Fig. 13, represent the tropics and extratropics (atmosphere + ocean mixed layer), with a boundary at 30° latitude, which is chosen

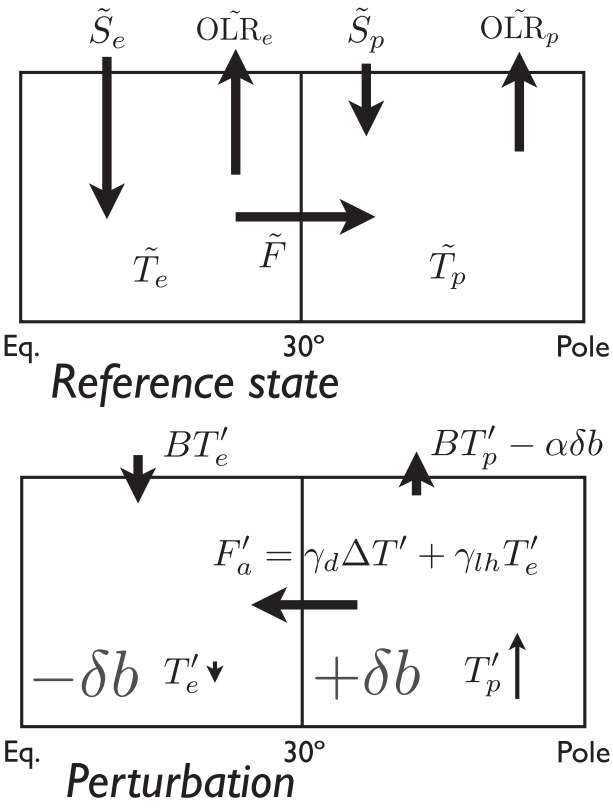

FIG. 13. Sketch of the two-box EBM. T_e and T_p represent tropical and extratropical sea surface temperatures. (top) A reference state with tropical excess in absorbed shortwave, $\tilde{S}_e > \tilde{S}_p$, balanced by both an OLR gradient and poleward heat transport $\tilde{F}$ (the net effect of AHT+OHT). (bottom) Response to heating anomalies δb mimicking an increase in OHT (tropical heat sink, extratropical heat source), balanced by anomalies in both OLR and AHT (we assume albedo is fixed). AHT parameterization includes contributions from DSE and LH. Polar OLR anomaly includes a term $-\alpha\delta b$ representing the convectively-driven increase in greenhouse trapping. Arrows indicate signs and relative magnitudes of changes following an increase in OHT: slight tropical cooling, large extratropical warming, and anomalous equatorward AHT. OLR anomalies are small everywhere: in the tropics, the temperature change is small, while in the extratropics the increase in emissions due to warming is mitigated by a decrease in emissions due to the more efficient greenhouse.

both for geometrical simplicity (i.e., both boxes have equal areas) and because our GCM is sensitive to OHT across 30°. The model is very crude, and is presented primarily to help clarify our thinking about the relative importance of heat transport and radiation processes in the proposed mechanism. We will show that the two-box model can be tuned to fit the GCM results quite well.

a. Formulation

Consider two well-mixed boxes with reference surface temperatures $\tilde{T}_e, \tilde{T}_p$. We suppose that this reference state involves a balance between the imposed equator-to-pole gradient in solar heating, the gradient in OLR, and some reference poleward heat flux $\tilde{F}$ (combined effect of AHT + OHT). We then introduce perturbations to the energy budget in each box $\delta b_e, \delta b_p$ and let the climate re-equilibrate. These perturbations might for example represent an increase in greenhouse gases or anomalous OHT (we consider both of these cases below). To simplify the problem, we suppose that the climate system adjusts to these forcings through changes in AHT and OLR, but that the solar forcing (i.e., the planetary albedo) is fixed. We thus have steady-state perturbation equations of the form

$$\delta b_e - F'_a = \mathrm{OLR}'_e \quad \delta b_p + F'_a = \mathrm{OLR}'_p. \tag{2}$$

Following LA07, perturbations in the AHT are parameterized as

$$F'_a = \gamma_d \Delta T' + \gamma_{\mathrm{lh}} T'_e, \tag{3}$$

with $\Delta T' = T'_e - T'_p$. We thus account for the different physics setting DSE and LH transports (Caballero and Langen 2005): DSE fluxes heat diffusively down the temperature gradient, while LH scales with the absolute temperature of the subtropical source regions feeding moisture into storm tracks. The parameters γ_d, γ_{lh} set the relative efficiency of these processes. LA07 offer plausible values $(\gamma_d, \gamma_{\mathrm{lh}}) = (1.6, 0.8)$ W m^{-2} °C^{-1}.

Typically in simple EBMs the OLR is assumed to be linear in temperature, e.g., $\mathrm{OLR}' = BT'$. We have argued that an additional longwave feedback is operating in the mid- to high latitudes: as heating at the sea surface from OHT convergence increases, there is an increase in convection within midlatitude storms, which drives an increase in greenhouse trapping and a reduction in OLR. A crude parameterization is simply

$$\mathrm{OLR}'_e = BT'_e \quad \text{and} \quad \mathrm{OLR}'_p = BT'_p - \alpha\delta b_p, \tag{4}$$

with α a dimensionless coefficient. A scaling for α in terms of more fundamental parameters can be obtained by invoking a model for the lapse rate and a convective adjustment constraint in the polar box (e.g., Abbot and Tziperman 2009). One supposes that an upward convective heat flux is required to maintain a moist adiabatic lapse rate; some fraction of δb_p is balanced by an increase in this convection, which in turn increases the optical thickness of the column, yielding the linearized expression (4). We skip this in the interest of simplicity.

b. A global mean heating

LA07 considered a uniform heating $\delta b_e = \delta b_p = \delta b$, for example, from an increase in greenhouse gases, and $\alpha = 0$. Solving the linear system with nonzero α gives

$$\overline{T}' = \frac{\delta b}{B}\left(1+\frac{\alpha}{2}\right) \quad \Delta T' = -\frac{\delta b}{\Gamma}\left[\frac{2\gamma_{\rm lh}}{B}\left(1+\frac{\alpha}{2}\right)+\alpha\right], \tag{5}$$

where we define $\Gamma = 2\gamma_d + \gamma_{\rm lh} + B$. Global mean temperature rises proportionally to the imposed heating, but it is accompanied by a reduction in ΔT—that is, the warming is polar-amplified, such that

$$\frac{\Delta T'}{\overline{T}'} = -\frac{2}{\Gamma}\left[\gamma_{\rm lh} + B\left(1+\frac{2}{\alpha}\right)^{-1}\right], \tag{6}$$

a constant ratio independent of the forcing δb. Climate changes in this model are always characterized by polar amplification. In the limit $\alpha \to 0$, we get LA07's result $\Delta T/\overline{T} = -2\gamma_{\rm lh}/\Gamma$, with the implication that polar amplification is intimately related to the efficiency of latent heat transport. In the present formulation, there is also a contribution from local longwave feedbacks in the polar box—the polar amplification increases with α.

One might be tempted to fit this result to $\Delta T/\overline{T} = -2.6$ as found in our GCM in Fig. 4. However this is the wrong scaling for experiments with altered OHT, since the forcings ought to be conservative (zero global mean). In the GCM, polar-amplified warming resulted not from a uniform radiative forcing but from a change in transport.

c. An imposed change in OHT

To mimic a change in OHT, we remove heat from the tropical box and deposit the same amount in the polar box, so that $\delta b_p = -\delta b_e$, as sketched in Fig. 13. Since this forcing represent anomalous OHT we will use the notation $\delta b_p = F'_o$. The solution becomes

$$\begin{aligned} T'_e &= -\frac{F'_o}{\Gamma}\left(1-\frac{\alpha\gamma_d}{B}\right) \\ T'_p &= +\frac{F'_o}{\Gamma}\left[1+\alpha\left(1+\frac{\gamma_d+\gamma_{\rm lh}}{B}\right)\right] \end{aligned} \tag{7}$$

or equivalently

$$\overline{T}' = \frac{\alpha F'_o}{2B} \quad \Delta T' = -\frac{2F'_o}{\Gamma}\left[1+\frac{\alpha}{2}\left(1+\frac{\gamma_{\rm lh}}{B}\right)\right]. \tag{8}$$

There can now only be a change in $\overline{T}$ due to an asymmetry in the atmospheric feedback between low and high latitudes. Let us first set $\alpha = 0$ to eliminate this asymmetry. In this case $\overline{T}' = 0$ and $\Delta T' = -2\Gamma^{-1}F'_o$, so that the increase in OHT leads to a flattening of the temperature gradient due to incomplete compensation by the AHT. To see this explicitly we can write the compensation as

$$\frac{F'_t}{F'_o} = \frac{F'_a + F'_o}{F'_o} = \frac{B}{\Gamma} = \frac{1}{1+\dfrac{2\gamma_d+\gamma_{\rm lh}}{B}} < 1, \tag{9}$$

where we define F'_t as the change in total (A+O) heat transport. In this case, OHT increases, the equator cools and the poles warm, with no change in $\overline{T}$. Perfect compensation occurs in this model in the high atmospheric efficiency limit $\gamma_d, \gamma_{\rm lh} \gg B$. In this limit the reduction in ΔT is very small, since the climate doesn't distinguish between AHT and OHT. This is at odds with our GCM results, in which F'_t/F'_o is small while $\Delta T'$ is not, and $\overline{T}$ also increases.

With nonzero α we can write the polar amplification as

$$\frac{\Delta T'}{\overline{T}'} = -\frac{2}{\Gamma}\left[\gamma_{\rm lh} + B\left(1+\frac{2}{\alpha}\right)\right]. \tag{10}$$

A component is thus driven by latent heat flux, but an additional contribution comes from the enhanced extratropical greenhouse effect, and significantly, would be nonzero even in the limit $\gamma_{\rm lh} \to 0$. LH transport is thus not an essential part of this mechanism. We can write the compensation of heat transport as

$$\frac{F'_t}{F'_o} = \frac{B}{\Gamma}\left(1-\frac{\alpha\gamma_d}{B}\right) \tag{11}$$

so that the THT perturbation decreases from its reference value in (9) proportionally to α (i.e., the atmosphere compensates more completely for the imposed OHT). The simultaneous reduction in ΔT and small-to-zero change in THT seen in the GCM demands that α be a positive $\mathcal{O}(1)$ quantity.

d. Perfect compensation and polar warming

At the critical value $\alpha = B/\gamma_d$, the perturbation in THT (11) goes to zero (perfect compensation), while from (7) the tropical temperature is unchanged ($T'_e = 0$), the pole warms by $T'_p = F'_o/\gamma_d$, and from (4) the OLR perturbations are zero. Polar warming is achieved without any change in the TOA radiative balance—in effect the polar box is in a local runaway greenhouse state (though the planet as a whole is not). The increase in OLR associated with the warming pole is exactly balanced by the reduction in OLR associated with the enhanced greenhouse; and the increase in poleward OHT is exactly balanced by a reduction in AHT associated with the weaker ΔT. There is no change in the latent heat component, since T_e does not change.

In this limit, the climate depends on the atmosphere–ocean partition of heat transport, while the TOA energy

balance does not. Our GCM apparently lies closer to this limit than to $\alpha = 0$. We also note that in the two-box model there is no contradiction between *decreased* total heat transport and polar warming; this is exactly what occurs with $\alpha > B/\gamma_d$. In this case the enhanced greenhouse effect is sufficiently large that the polar OLR decreases, and the tropics warm slightly from the decrease in poleward heat transport.

e. Quantitative estimates

We estimate α from our GCM by noting that $\overline{T}$ varies by 5°C over a 3 PW range in OHT, or 0.21°C (W m^{-2})$^{-1}$ convergence in the polar box. We fit to (8) with B = 2 W m^{-2} °C^{-1} (North et al. 1981) to find $\alpha = 0.84$. Taking the above values from LA07 for γ_d, $\gamma_{\rm lh}$, we then use (10) to estimate $\Delta T/\overline{T} = -2.5$ for the two-box model—very close to the corresponding value −2.6 from the GCM.

With this parameter set we have $\alpha\gamma_d/B = 0.67$, not far from the perfect compensation limit. From (11) we find $F_t'/F_o' = 0.11$, that is, the total heat transport increases by just 11% of the imposed increase in OHT. This is consistent with the GCM results shown in Fig. 6: roughly 0.2 PW variation in THT for a 3 PW variation in OHT. The two-box model thus captures the simultaneous strong polar warming and near-perfect compensation of heat transport that occurs in the GCM.

These estimates are insensitive to the latent heat flux. Setting $\gamma_{\rm lh} = 0$ gives $F_t'/F_o' = 0.13$, $\Delta T/\overline{T} = -2.6$. This insensitivity stems from the fact that tropical temperatures (which set the latent heat transport) do not vary much in these solutions, since the model is close to the perfect compensation limit. If the AHT efficiency were doubled to $(\gamma_d, \gamma_{\rm lh})$ = (3.2, 1.6) W m^{-2} °C^{-1}, the model would be in the ''over-compensating'' regime with $\alpha\gamma_d/B = 1.3$. This would yield a negative perturbation in total heat transport $F_t'/F_o' = -0.23$ and a weaker polar amplification, $\Delta T/\overline{T} = -1.3$.

5. Discussion

We have shown that an increase in OHT leads to a global warming and flattening of the surface temperature gradient in a GCM with simple aquaplanet geometry. The key new result of this paper is the clear demonstration that the large reductions in ΔT take place in spite of efficient compensation by the atmosphere, and are not driven by an increase in total poleward heat transport. Low-latitude OHT instead affects the climate through a modulation of the water vapor greenhouse properties of the extratropical atmosphere.

Within the confines of this particular model, then, the scenario laid out in the introduction is correct. We summarize the mechanism by which an increase in OHT leads to polar-amplified warming as follows: the hypothesized increase in OHT takes heat out of the Hadley cell regime and deposits heat under the influence of the midlatitude storm track. The tropical circulation adjusts through a combination of cloud effects and circulation changes to keep tropical SST changes small. Meanwhile there is an increase in the heating of the midlatitude sea surface and a decrease in the heating from AHT convergence aloft. This heating pattern destabilizes midlatitude storms, which respond by increasing the frequency of deep moist convection and decreasing the stable large-scale precipitation. Increased convection injects warm moist air into the upper troposphere, increasing the relative humidity at high levels where it is most radiatively active. The surface is ultimately kept warmer by the resulting increase in downwelling longwave radiation. The warming stretches to the poles despite the shorter reach of the imposed OHT anomaly, because atmospheric transport processes efficiently bridge the gap between mid and high latitudes. We have not explicitly addressed the fact that the surface warming peaks at the poles in all cases, but we suspect that the positive cloud feedback during polar night described by Abbot and Tziperman (2008a) plays a key role in this local maximum.

These results offer a straightforward potential resolution to the low-gradient paradox. OHT is very effective at warming the mid- to high latitudes, while ineffective at cooling the tropics. Large variations in surface temperature gradient are possible without substantial changes in TOA radiative balance. In effect, the surface temperature gradient is not linked to the total heat transport, but rather to its partitioning between the atmosphere and ocean.

There are of course many caveats to the above scenario. There is no evidence that past variations in OHT were as large as the 3 PW range sampled in our experiments. The aquaplanet geometry limits any direct application to specific paleoclimate questions. The moist physics in the atmospheric model is highly parameterized, and yet these moist processes are critical components of the proposed mechanism. It is clearly desirable to test out these ideas in models with more sophisticated physics, as well as models with more realistic configurations. It is our hope that these results will spur further investigation of the indirect role played by OHT in setting the greenhouse properties of the atmosphere.

We have tested the sensitivity of our results to parameter values in the GCM's moist convection scheme; see the appendix and Fig. 14. Quantitative details of the climate response to OHT are sensitive to the entrainment parameter. This is consistent with a number of

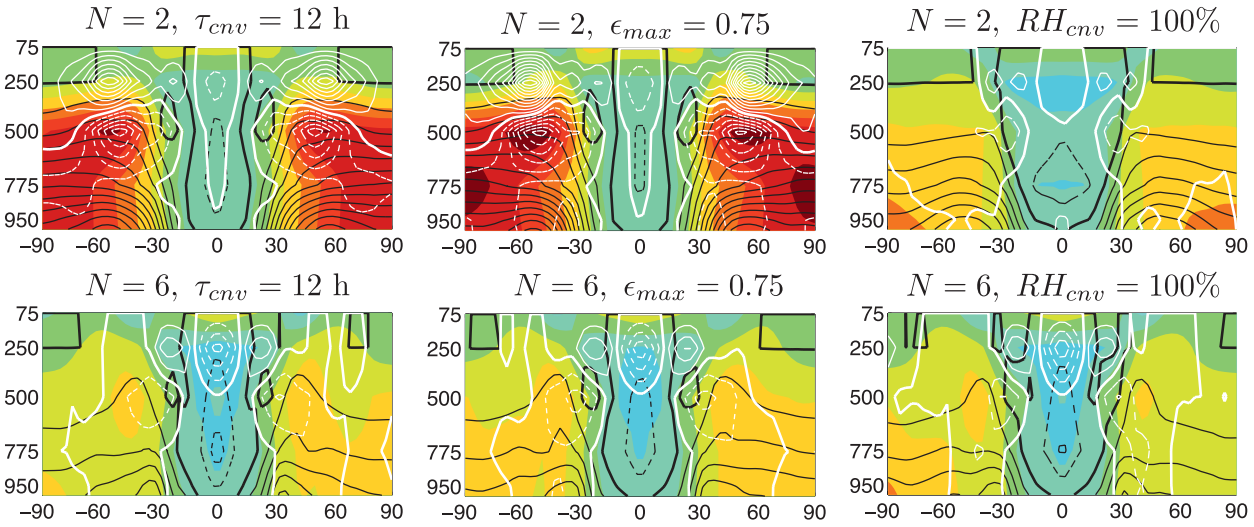

FIG. 14. Sensitivity tests with perturbed convection scheme parameters. Anomalies of temperature (colors), specific (black) and relative humidity (white) as OHT increases from 2 to 3 PW. Same color scale and contour intervals as in Fig. 12. Reference parameter values are $\tau_{cnv} = 6$ h, $\epsilon_{max} = 0.5$ and $RH_{cnv} = 80\%$.

recent studies identifying convective entrainment exerting an outsized influence on the properties of GCMs (e.g., Held et al. 2007; Sanderson et al. 2008; Kang et al. 2008, 2009). On the other hand, our tests show that the warming mechanism is quite robust in a qualitative sense to large changes in convective parameters. The spatial patterns of warming and relative moistening/drying in Fig. 12 are reproduced in all our tests, unless convection is explicitly (and unphysically) suppressed. In one test in which the convection scheme cannot activate outside of the warm tropics, the upper-tropospheric relative moistening and associated strong greenhouse trapping in response to increased OHT does not occur. This confirms the central role of extratropical convection in the warming mechanism.

An important aspect of the "equable climate problem" (Huber and Caballero 2011) is evidence for warm winters in the interior of high-latitude continents. A long-standing objection to the "enhanced OHT" hypothesis (e.g., Barron 1987), is that while strong OHT is effective at warming the sea surface, it also tends to generate more sluggish atmospheric circulation, leading to a cooling of continental interiors. For this reason, it is sometimes argued that the early Eocene must have had reduced OHT (e.g., Bice et al. 2000). While our results obviously do not deal directly with the question of continental climates, they do offer some useful insight into this problem. In our model, the poles are kept warm through atmospheric processes, and in all cases but $N = 1$, there is in fact a vigorous atmospheric circulation from mid- to high latitudes. We speculate that high-latitude continents could be kept warm through advection of upper tropospheric water vapor, so long as sufficient deep convection were to be triggered within the oceanic storm tracks. On the other hand, localized sea surface heating can induce upstream cooling over adjacent continents by a purely dynamical mechanism (Kaspi and Schneider 2011). Future work will focus on the impact of OHT variations and convective moistening in the presence of land/ocean contrast.

Our results are suggestive of two distinct and additive warming effects, though both mechanisms involve modulations of moist convection. One operates in the tropics/subtropics and is tied to the Hadley cells, the other in the midlatitudes tied to storm tracks. Shifting from high to low N emphasizes one or the other mechanism. In our GCM, the strongest global warming signals are found in cases with small N where the forcing is able to interact strongly with storm tracks. For large N we find only modest warming despite large perturbations in the tropical/subtropical distribution of cloud, precipitation and water vapor, a result we have attributed at least in part to close cancellation between short- and longwave effects of cloud changes. We speculate that the relative warming efficiency of the two mechanisms may vary substantially from model to model with different treatments of clouds and convection. The outlier case $N = 1$ may also point to a third warming effect, this one local to the high latitudes, in which the positive feedback described by Abbot and Tziperman (2008a) comes to the fore.

We have not focused on the hydrological balance; however, the substantial decrease in subtropical net evaporation with warming in Fig. 10 demands explanation. As noted above, Held and Soden (2006) find a robust (though 5 × weaker) increase in subtropical $E - P$

in models of twenty-first century global warming. We surmise at least two reasons for this discrepancy. First, the Held and Soden scaling seems to break down in the very warm, weak ΔT regime. In a suite of gray-radiation GCM simulations with zero OHT, O'Gorman and Schneider (2008) find that subtropical precipitation rate is rather insensitive to greenhouse warming for climates near the present-day reference, but increases sharply for $\overline{T} > 310$ K (largely from convective rain). The authors loosely attribute this to a reorganization of meridional moisture fluxes as tropical-extratropical Q gradients weaken, with more subtropical evaporation balanced locally by precipitation. Secondly, increased OHT projects strongly onto reduced Hadley cell mass flux (e.g., Levine and Schneider 2011), weakening the subtropical downwelling. There is therefore less of a barrier to destabilization of the subtropical atmosphere under increased OHT. Our simulations are consequently within the regime of decreasing subtropical $E - P$ (due to rapidly increasing convective rain) with warming at cooler $\overline{T}$ than reported by O'Gorman and Schneider (2008). The $E - P$ signal plotted in Fig. 10 is large, and suggests that past variations in OHT could be estimated from geological evidence of subtropical hydrology such as sedimentation from river runoff or evaporite deposits. However the above discussion is very speculative, and the dynamics underlying the transition to convectively active subtropics require further study.

The very simple scaling of $\overline{T}$ and ΔT in Fig. 4, together with the overall insensitivity of the model climate to the details of the meridional structure of OHT, suggests an interesting universality to potential climate changes, as discussed by Lindzen (1994). It may not be possible to change $\overline{T}$ without changing ΔT, and vice-versa; in other words, polar amplification may be a fundamental feature of all climate changes. Of course this result could well be an artifact of the simplicity of the model setup used here, including our limited focus on equilibrium climates. Still, it is an intriguing possibility that warrants further investigation.

6. Conclusions

In reference to the key questions posed in the introduction, we conclude the following.

(i) An increase in either amplitude or meridional scale of OHT leads to a polar-amplified global mean warming: increase in $\overline{T}$ and decrease in ΔT.
(ii) Polar warming results from any increase in OHT across 30°, beyond the Hadley cell regime, but is insensitive to the detailed meridional structure of the convergence. Direct OHT into the high latitudes is not a prerequisite for an ice-free pole.
(iii) Changes in OHT out of the tropics impact the climate primarily through modulation of deep moist convection within midlatitude storm tracks.
(iv) The warming results from an enhanced water vapor greenhouse, accompanying the midlatitude shift to convective precipitation.
(v) Polar warming occurs without any increase in THT. The enhanced extratropical greenhouse allows for an increase in surface temperatures with no change in OLR.

Our findings have potentially important consequences for our understanding of past warm climates. The climatic impact of OHT depends primarily on its gross features (transport across 30°), and not on subtle details on the meridional structure. Mechanisms such as continental drift that modulate the efficiency of OHT out of the tropics will be felt at the poles, regardless of the details of the extratropical ocean circulation. There are also important consequences for numerical modeling of warm climates. Threshold values for forcings such as CO_2 for the maintenance of warm poles may be strongly dependent on the OHT (or lack thereof). Given the importance of moist convection to the warming mechanism, differences in convection schemes may also turn out to be an important element.

We emphasize the caveat that our conclusions are based on a rather crude model. The proposed mechanism awaits verification in more comprehensive GCMs with a range of different parameterizations of moist processes. These efforts are currently underway.

Acknowledgments. BR received funding from a NOAA Climate Climate and Global Change Postdoctoral Fellowship, administered by the University Corporation for Atmospheric Research. DF acknowledges support of the Physical Oceanography program of NSF. We are grateful for helpful discussions with J. Marshall, D. Battisti, A. Czaja, C. Bitz, A. Donohoe, T. Schneider, P. O'Gorman, A. Plumb, D. Frierson and D. Schrag. We thank the editor Anthony Broccoli and three anonymous reviewers for helpful comments.

APPENDIX

Convection Scheme and Sensitivity Tests

a. Description of the moist convection scheme

The moist convection code in our GCM is adapted from SPEEDY. It is fully documented in the appendix to Molteni (2003) (available at http://users.ictp.it/~kucharsk/speedy_description/molteni2002_appendixA.pdf). We

give a brief overview here, following Molteni's notation closely.

The scheme is activated wherever saturation moist static energy decreases with height, and one of two threshold conditions on boundary layer humidity Q is met:

$$Q > Q_{\text{thr}} = \min(Q_{\text{cnv}}, \text{RH}_{\text{cnv}} Q^{\text{sat}}), \qquad \text{(A1)}$$

where Q^{sat} is the boundary layer saturation specific humidity and Q_{cnv}, RH_{cnv} are convective threshold values for specific and relative humidity respectively. Upward and downward fluxes of moisture and DSE can then be defined relative to a cloud base mass flux F^*. The scheme is closed by treating the Q tendency as a relaxation toward Q_{thr}:

$$\left(\frac{\partial Q}{\partial t}\right)_{\text{cnv}} = -\frac{Q - Q_{\text{thr}}}{\tau_{\text{cnv}}}, \qquad \text{(A2)}$$

which determines F^* in terms of the vertical structure of moisture and temperature. Above the boundary layer the upward mass flux is increased by a factor ϵ due to entrainment. The prescribed entrainment profile decreases from ϵ_{max} at the surface to zero at 500 hPa. All detrainment is assumed to occur at cloud top. The effects of condensation and latent heat release therefore need only be calculated at cloud top, where convective precipitation is computed from the updraft supersaturation. Net tendencies for moisture and DSE can then be computed for every tropospheric layer. Standard parameter values are $Q_{\text{cnv}} = 15$ g kg^{-1}, $\text{RH}_{\text{cnv}} = 80\%$, $\tau_{\text{cnv}} = 6$ h, and $\epsilon_{\text{max}} = 0.5$.

b. Sensitivity tests

We perform several sensitivity tests with altered convective parameters. For each test, we integrate the model out to equilibrium with four different OHT profiles: $N = 2$ (2 PW, 3 PW) and $N = 6$ (2 PW, 3 PW). These are chosen to highlight the relative importance of the tropical versus extratropical responses to changes in OHT amplitude, which are strong for $N = 6$ and $N = 2$ respectively (see the greenhouse trapping in Fig. 9 and the RH anomalies in Fig. 12).

One set of tests alters the relaxation rate of boundary layer humidity by doubling or halving τ_{cnv}. Another set alters the entrainment flux by increasing/decreasing ϵ_{max}. These tests do not distinguish between tropical and extratropical convection. Finally we increase the relative humidity threshold RH_{cnv} to 100%, which selectively eliminates extratropical convection. This is because Q is typically above 15 g kg^{-1} wherever the SST is sufficiently warm; in the vast majority of our runs this condition is met everywhere equatorward of 30°, and out to 40°–50° in a few warmer runs. Convection over cooler extratropical oceans instead requires that $\text{RH} > \text{RH}_{\text{cnv}}$; by setting the threshold to 100% we prevent it entirely (since the large-scale condensation scheme relaxes saturated boundary layer air back to 90% RH) while maintaining convection in the warm tropics. This test is unphysical but confirms the key importance of extratropical convection to the warming mechanism.

TABLE A1. Change in greenhouse trapping $\Delta\overline{G_t}$ averaged poleward of 30°N, for a 1 PW increase in OHT (in W m^{-2}). Values in parentheses are deviations from the reference case. Reference parameter values are $\text{RH}_{\text{cnv}} = 80\%$, $\tau_{\text{cnv}} = 6$ h, $\epsilon_{\text{max}} = 0.5$. The spatial structure of ΔG_t is plotted in Fig. 9 for the reference cases.

Experiment	$N = 2$	$N = 6$
Reference	18.3	8.3
$\tau_{\text{cnv}} = 12$ h	19.0 (+0.7)	8.4 (+0.1)
$\tau_{\text{cnv}} = 3$ h	19.1 (+0.8)	8.2 (−0.1)
$\epsilon_{\text{max}} = 0.75$	21.9 (+3.6)	10.8 (+2.5)
$\epsilon_{\text{max}} = 0.25$	15.9 (−2.4)	6.6 (−1.7)
$\text{RH}_{\text{cnv}} = 100\%$	11.0 (−7.3)	6.5 (−1.8)

We summarize the results in Table A1 in terms of the anomaly in extratropical greenhouse trapping $\Delta\overline{G_t}$ (averaged poleward of 30°) for an increase in OHT from 2 to 3 PW. We showed in Fig. 10 that $\overline{G_t}$ is very well correlated with $\overline{T}$ (and therefore also with ΔT), and argued that changes in greenhouse trapping are in fact driving the warming. Results are very insensitive to τ_{cnv}. There is some sensitivity to entrainment rate ϵ_{max}; more entrainment leads to a heightened sensitivity to OHT variations, both for $N = 2$ and $N = 6$. By far the largest perturbation occurs in the case $N = 2$, $\text{RH}_{\text{cnv}} = 100\%$. Here, by suppressing all extratropical convection the change in greenhouse trapping is reduced by nearly a factor of 2 from its reference value. The case $N = 6$ is much less sensitive to the suppression of extratropical convection, which is consistent with the small extratropical convective response in the reference case for $N = 6$ (e.g., Figure 11).

Figure 14 shows the spatial structures of temperature/moisture anomalies for a subset of these perturbed physics runs. The cases with $\tau_{\text{cnv}} = 12$ h look nearly identical to the reference cases in Fig. 12, consistent with the very weak perturbations in greenhouse trapping in Table A1. The runs with enhanced entrainment show somewhat more intense versions of the reference warming/moistening patterns in Fig. 12, particularly for the case $N = 2$. Peak upper level relative moistening for $N = 2$ increases from about 15% in the reference case to 20% for $\epsilon_{\text{max}} = 0.75$. In sharp contrast, the extratropical RH dipole (upper moistening, midlevel drying) is entirely absent from the cases with $\text{RH}_{\text{cnv}} = 100\%$, and the

warming pattern for $N = 2$ is markedly less intense. This is fully consistent with the warming being largely driven by extratropical convective moistening in the reference case.

REFERENCES

Abbot, D. S., and E. Tziperman, 2008a: A high-latitude convective cloud feedback and equable climates. *Quart. J. Roy. Meteor. Soc.,* **134,** 165–185.

——, and ——, 2008b: Sea ice, high-latitude convection, and equable climates. *Geophys. Res. Lett.,* **35,** L03702, doi:10.1029/2007GL032286.

——, and ——, 2009: Controls on the activation and strength of a high-latitude convective cloud feedback. *J. Atmos. Sci.,* **66,** 519–529.

——, M. Huber, G. Bousquet, and C. C. Walker, 2009a: High-CO_2 cloud radiative forcing feedback over both land and ocean in a global climate model. *Geophys. Res. Lett.,* **36,** L05702, doi:10.1029/2008GL036703.

——, C. C. Walker, and E. Tziperman, 2009b: Can a convective cloud feedback help to eliminate winter sea ice at high CO_2 concentrations? *J. Climate,* **22,** 5719–5731.

Adcroft, A., J.-M. Campin, C. Hill, and J. Marshall, 2004: Implementation of an atmosphere–ocean general circulation model on the expanded spherical cube. *Mon. Wea. Rev.,* **132,** 2845–2863.

Barron, E. J., 1983: A warm, equable Cretaceous: the nature of the problem. *Earth Sci. Rev.,* **19,** 305–338.

——, 1987: Eocene equator-to-pole surface ocean temperatures: A significant climate problem? *Paleoceanography,* **2,** 729–739.

——, W. H. Peterson, D. Pollard, and S. Thompson, 1993: Past climate and the role of ocean heat transport: Model simulations for the Cretaceous. *Paleoceanography,* **8,** 785–798.

Bice, K. L., C. R. Scotese, D. Seidov, and E. J. Barron, 2000: Quantifying the role of geographic change in Cenozoic ocean heat transport using uncoupled atmosphere and ocean models. *Palaeogeogr. Palaeoclimatol. Palaeoecol.,* **161,** 295–310.

Bracco, A., F. Kucharski, R. Kallummal, and F. Molteni, 2004: Internal variability, external forcing and climate trends in multi-decadal AGCM ensembles. *Climate Dyn.,* **23,** 659–678.

Bush, A. B., and S. G. H. Philander, 1997: The late Cretaceous: Simulation with a coupled atmosphere-ocean general circulation model. *Paleoceanography,* **12,** 495–516.

Caballero, R., and P. L. Langen, 2005: The dynamic range of poleward energy transport in an atmospheric general circulation model. *Geophys. Res. Lett.,* **32,** L02705, doi:10.1029/2004GL021581.

Clement, A. C., R. Seager, M. A. Cane, and S. E. Zebiak, 1996: An ocean dynamical thermostat. *J. Climate,* **9,** 2190–2196.

Covey, C., and E. Barron, 1988: The role of ocean heat transport in climatic change. *Earth Sci. Rev.,* **24,** 429–445.

Czaja, A., and J. Marshall, 2006: The partitioning of poleward heat transport between the atmosphere and ocean. *J. Atmos. Sci.,* **63,** 1498–1511.

——, and N. Blunt, 2011: A new mechanism for ocean–atmosphere coupling in midlatitudes. *Quart. J. Roy. Meteor. Soc.,* **137,** 1095–1101.

D'Hondt, S., and M. A. Arthur, 1996: Late Cretaceous oceans and the cool tropic paradox. *Science,* **271,** 1838–1841.

Emanuel, K., 2002: A simple model of multiple climate regimes. *J. Geophys. Res.,* **107,** 4077, doi:10.1029/2001JD001002.

Enderton, D., and J. Marshall, 2009: Explorations of atmosphere-ocean-ice climates on an aquaplanet and their meridional energy transports. *J. Atmos. Sci.,* **66,** 1593–1611.

Ferreira, D., J. Marshall, and J.-M. Campin, 2010: Localization of deep water formation: Role of atmospheric moisture transport and geometrical constraints on ocean circulation. *J. Climate,* **23,** 1456–1476.

——, ——, and B. E. J. Rose, 2011: Climate determinism revisited: multiple equilibria in a complex climate model. *J. Climate,* **24,** 992–1012.

Greenwood, D. R., and S. L. Wing, 1995: Eocene continental climates and latitudinal temperature gradients. *Geology,* **23,** 1044–1048.

Hazeleger, W., R. Seager, M. A. Cane, and N. H. Naik, 2004: How can tropical Pacific ocean heat transport vary? *J. Phys. Oceanogr.,* **34,** 320–333.

Held, I. M., 2001: The partitioning of the poleward energy transport between the tropical ocean and atmosphere. *J. Atmos. Sci.,* **58,** 943–948.

——, and B. J. Soden, 2006: Robust responses of the hydrological cycle to global warming. *J. Climate,* **19,** 5686–5699.

——, M. Zhao, and B. Wyman, 2007: Dynamic radiative–convective equilibria using GCM column physics. *J. Atmos. Sci.,* **64,** 228–238.

Herweijer, C., R. Seager, M. Winton, and A. Clement, 2005: Why ocean heat transport warms the global mean climate. *Tellus,* **57A,** 662–675.

Hotinski, R., and J. Toggweiler, 2003: Impact of a Tethyan circumglobal passage on ocean heat transport and "equable" climates. *Paleoceanography,* **18,** 1007, doi:10.1029/2001PA000730.

Huber, M., 2008: A hotter greenhouse? *Science,* **321,** 353–354.

——, and L. C. Sloan, 2000: Climatic responses to tropical sea surface temperature changes on a "greenhouse" Earth. *Paleoceanography,* **15,** 443–450.

——, and ——, 2001: Heat transport, deep waters, and thermal gradients: Coupled simulation of an Eocene greenhouse climate. *Geophys. Res. Lett.,* **28,** 3481–3484.

——, and D. Nof, 2006: The ocean circulation in the Southern Hemisphere and its climate impacts in the Eocene. *Palaeogeogr. Palaeoclimatol. Palaeoecol.,* **231,** 9–28.

——, and R. Caballero, 2011: The early Eocene equable climate problem revisited. *Climate Past,* **7,** 603–633.

——, L. C. Sloan, and C. Shellito, 2003: Early Paleogene oceans and climate: A fully coupled modeling approach using the NCAR GCM. *Causes and Consequences of Globally Warm Climates in the Early Paleogene,* S. L. Wing et al., Eds., Geology Society of America, 25–47.

Jansen, M., and R. Ferrari, 2009: Impact of the latitudinal distribution of tropical cyclones on ocean heat transport. *Geophys. Res. Lett.,* **36,** L06604, doi:10.1029/2008GL036796.

——, ——, and T. A. Mooring, 2010: Seasonal versus permanent thermocline warming by tropical cyclones. *Geophys. Res. Lett.,* **37,** L03602, doi:10.1029/2009GL041808.

Kang, S. M., I. M. Held, D. M. W. Frierson, and M. Zhao, 2008: The response of the ITCZ to extratropical thermal forcing: Idealized slab-ocean experiments with a GCM. *J. Climate,* **21,** 3521–3532.

——, D. M. W. Frierson, and I. M. Held, 2009: The tropical response to extratropical thermal forcing in an idealized GCM: The importance of radiative feedbacks and convective parameterization. *J. Atmos. Sci.,* **66,** 2812–2827.

Kaspi, Y., and T. Schneider, 2011: Winter cold of eastern continental boundaries induced by warm ocean waters. *Nature,* **471,** 621–624.

Korty, R. L., and K. A. Emanuel, 2007: The dynamic response of the winter stratosphere to an equable climate surface temperature gradient. *J. Climate,* **20,** 5213–5228.

——, and T. Schneider, 2007: A climatology of the tropospheric thermal stratification using saturation potential vorticity. *J. Climate,* **20,** 5977–5991.

——, K. A. Emanuel, and J. R. Scott, 2008: Tropical cyclone–induced upper-ocean mixing and climate: Application to equable climates. *J. Climate,* **21,** 638–654.

Langen, P. L., and V. A. Alexeev, 2007: Polar amplification as a preferred response in an idealized aquaplanet GCM. *Climate Dyn.,* **29,** 305–317.

Levine, X., and T. Schneider, 2011: Response of the Hadley circulation to climate change in an aquaplanet GCM coupled to a simple representation of ocean heat transport. *J. Atmos. Sci.,* **68,** 769–783.

Lindzen, R. S., 1994: Climate dynamics and global change. *Annu. Rev. Fluid Mech.,* **26,** 353–378.

Manabe, S., 1969: Climate and the ocean circulation II. The atmospheric circulation and the effects of heat transfer by ocean currents. *Mon. Wea. Rev.,* **97,** 775–805.

Marshall, J., A. Adcroft, C. Hill, L. Perelman, and C. Heisey, 1997: A finite-volume, incompressible Navier Stokes model for studies of the ocean on parallel computers. *J. Geophys. Res.,* **102,** 5753–5766.

——, ——, J.-M. Campin, C. Hill, and A. White, 2004: Atmosphere-ocean modeling exploiting fluid isomorphisms. *Mon. Wea. Rev.,* **132,** 2882–2894.

——, D. Ferreira, J.-M. Campin, and D. Enderton, 2007: Mean climate and variability of the atmosphere and ocean on an aquaplanet. *J. Atmos. Sci.,* **64,** 4270–4286.

Minobe, S., A. Kuwano-Yoshida, N. Komori, S.-P. Xie, and R. J. Small, 2008: Influence of the Gulf Stream on the troposphere. *Nature,* **452,** 206–209.

Molteni, F., 2003: Atmospheric simulations using a GCM with simplified physical parameterizations. I: model climatology and variability in multi-decadal experiments. *Climate Dyn.,* **20,** 175–191.

Norris, R. D., K. L. Bice, E. A. Magno, and P. A. Wilson, 2002: Jiggling the tropical thermostat in the Cretaceous hothouse. *Geology,* **30,** 299–302.

North, G. R., R. F. Cahalan, and J. A. Coakley, 1981: Energy balance climate models. *Rev. Geophys. Space Phys.,* **19,** 91–121.

O'Gorman, P. A., and T. Schneider, 2008: The hydrological cycle over a wide range of climates simulated with an idealized GCM. *J. Climate,* **21,** 3815–3832.

Otto-Bliesner, B. L., E. C. Brady, and C. Shields, 2002: Late Cretaceous ocean: Coupled simulations with the National Center for Atmospheric Research Climate System Model. *J. Geophys. Res.,* **107,** 4019, doi:10.1029/2001JD000821.

Pearson, P. N., B. E. van Dongen, C. J. Nicholas, R. D. Pancost, S. Schouten, J. M. Singano, and B. S. Wade, 2007: Stable warm tropical climate through the Eocene Epoch. *Geology,* **35,** 211–214.

Pierrehumbert, R. T., 2002: The hydrologic cycle in deep-time climate problems. *Nature,* **419,** 191–198.

——, 2010: *Principles of Planetary Climate.* Cambridge University Press, 680 pp.

——, H. Brogniez, and R. Roca, 2007: On the relative humidity of the atmosphere. *The Global Circulation of the Atmosphere,* T. Schneider and A. H. Sobel, Eds., Princeton University Press, 143–185.

Rind, D., and M. Chandler, 1991: Increased ocean heat transports and warmer climates. *J. Geophys. Res.,* **96,** 7437–7461.

Rose, B. E. J., and J. Marshall, 2009: Ocean heat transport, sea ice, and multiple climate states: Insights from energy balance models. *J. Atmos. Sci.,* **66,** 2828–2843.

Royer, D. L., R. A. Berner, I. P. Montañez, N. J. Tabor, and D. J. Beerling, 2004: CO_2 as a primary driver of Phanerozoic climate. *GSA Today,* **14,** 4–10.

Sanderson, B., C. Piani, W. Ingram, D. Stone, and M. Allen, 2008: Towards constraining climate sensitivity by linear analysis of feedback patterns in thousands of perturbed-physics GCM simulations. *Climate Dyn.,* **30,** 175–190.

Schmidt, G. A., and L. A. Mysak, 1996: Can increased poleward oceanic heat flux explain the warm Cretaceous climate? *Paleoceanography,* **11,** 579–593.

Seager, R., D. Battisti, J. Yin, N. Gordon, N. Naik, A. Clement, and M. Cane, 2002: Is the Gulf Stream responsible for Europe's mild winters? *Quart. J. Roy. Meteor. Soc.,* **128,** 2563–2586.

Severijns, C. A., and W. Hazeleger, 2010: The efficient global primitive equation climate model SPEEDO V2.0. *Geosci. Model Dev.,* **3,** 105–122.

Sloan, L. C., J. C. G. Walker, and T. C. M. Jr, 1995: Possible role of oceanic heat transport in early Eocene climate. *Paleoceanography,* **10,** 347–356.

Sobel, A. H., 2001: The weak temperature gradient approximation and balanced tropical moisture waves. *J. Atmos. Sci.,* **58,** 3650–3665.

Stone, P. H., 1978: Constraints on dynamical transports of energy on a spherical planet. *Dyn. Atmos. Oceans,* **2,** 123–139.

Tiedtke, M., 1989: A comprehensive mass flux scheme for cumulus parameterization in large-scale models. *Mon. Wea. Rev.,* **117,** 1779–1800.

Trenberth, K. E., and J. M. Caron, 2001: Estimates of meridional atmosphere and ocean heat transports. *J. Climate,* **14,** 3433–3443.

Vallis, G. K., and R. Farneti, 2009: Meridional energy transport in the coupled atmosphere–ocean system: Scaling and numerical experiments. *Quart. J. Roy. Meteor. Soc.,* **135,** 1643–1660.

von der Heydt, A., and H. A. Dijkstra, 2006: Effect of ocean gateways on the global ocean circulation in the late Oligocene and early Miocene. *Paleoceanography,* **21,** PA1011, doi:10.1029/2005PA001149.

Wilson, P. A., R. D. Norris, and M. J. Cooper, 2002: Testing the Cretaceous greenhouse hypothesis using glassy foraminiferal calcite from the core of the Turonian tropics on Demerara Rise. *Geology,* **30,** 607–610.

Winton, M., 2003: On the climatic impact of ocean circulation. *J. Climate,* **16,** 2875–2889.

Wunsch, C., 2005: The total meridional heat flux and its oceanic and atmospheric partition. *J. Climate,* **18,** 4374–4380.

Zachos, J., M. Pagani, L. Sloan, E. Thomas, and K. Billups, 2001: Trends, rhythms, and aberrations in global climate 65 Ma to present. *Science,* **292,** 686–693.

Zhang, Z., K. Nisancioglu, F. Flatøy, M. Bentsen, I. Bethke, and H. Wang, 2011: Tropical seaways played a more important role than high latitude seaways in Cenozoic cooling. *Climate Past,* **7,** 801–813.

Zhou, J., C. Poulsen, D. Pollard, and T. White, 2008: Simulation of modern and middle Cretaceous marine $\delta^{18}O$ with an ocean-atmosphere general circulation model. *Paleoceanography,* **23,** PA3223, doi:10.1029/2008PA001596.